EGG-NE--10263

DE92 018052

Safety Rod / Thimble Melt Failure Characterization Experiments

Carl M. Stoots
Grant Hawkes

May, 1992

Idaho National Engineering Laboratory
EG&G Idaho, Inc.
P.O. Box 1625
Idaho Falls, ID 83415-2404

Prepared for the U.S. Department of Energy
Assistant Secretary for Nuclear Energy
Under DOE Idaho Field Office
Contract No. DE-AC07-76ID01570

Safety Rod / Thimble Melt Failure Characterization Experiments

Prepared by:

C. M. Stoots — 5/11/92 (Date)

G. L. Hawkes — 5/11/92 (Date)

Approved by:

W. G. Lussie — 5/11/92 (Date)

D. C. Mecham — 5/11/92 (Date)

ABSTRACT

The Department of Energy (DOE) requested that the INEL perform experiments to study the thermal failure characteristics of a simulated Savannah River Site nuclear reactor safety rod and its surrounding thimble assembly. An electrically heated stainless steel rod simulated a reactor safety rod located eccentrically or concentrically within a perforated aluminum guide tube or thimble. A total of 37 experiments were conducted for a range of power levels and safety rod / thimble relative orientations. Video tapes were made of the four failure tests that were conducted to the melting point of the thimble. Although the primary emphasis of the experiments were to characterize the melting of the thimble qualitatively, experimental transient measurements included heater voltage and current, heater surface temperatures, aluminum thimble temperatures, and ambient temperature. Numerical studies were also performed in support of the experiments and data interpretation. Two finite element models were created to model the heat conduction-radiation between the stainless steel heater and thimble. The predicted temperatures were in good agreement with the experimental results.

EXECUTIVE SUMMARY

Steady state and transient heat transfer experiments were conducted to study a simulated Savannah River Site (SRS) reactor safety rod in contact with an aluminum guide tube (thimble) while undergoing heating due to gamma energy absorption. Electrical resistance heating was used to simulate the gamma heating. The simulated safety rod and thimble duplicated the SRS safety rod / thimble geometry. The outer diameter of the simulated safety rod was 2.39 cm. The thimbles used were sections of actual SRS reactor thimbles with an average inner diameter of 2.72 cm and average wall thickness of 2.54 mm. The heated length of the simulated safety rod was approximately 68.6 cm. Thimble sections were 60.96 cm in length. Measurements were made for safety rod power levels ranging from 26 to 1843 watts/m. Three melt failure tests were performed with the safety rod in contact with the thimble, while one melt failure test was performed with the safety rod centered within the thimble. Transient measurements included simulated safety rod voltage and current, safety rod skin temperatures, thimble temperatures, and ambient temperature. Video tapes were made of the four melt tests conducted.

The primary objective of these experiments was to provide qualitative information concerning the mode and severity of failure by melting of an aluminum thimble in contact with a SRS safety rod. This information is necessary to estimate the maximum safety rod temperatures a thimble can sustain before melting. To support this objective, these experiments were designed to provide qualitative, and limited quantitative, data on the effects of combined thermal conduction, convection, and thermal radiation upon an aluminum thimble in contact with a SRS safety rod undergoing gamma heating after a hypothesized loss of coolant accident.

Results indicated that for the conditions of these specific experiments thimble melt failure occurs at safety rod power levels of approximately 1380 watts/m or higher. Corresponding safety rod and thimble temperatures at failure were on the order of 860 C and 620 C, respectively. The mode of thimble failure by melting was fairly benign. Typically, molten aluminum would flow to a cooler thimble location and resolidify. In some cases a small quantity of molten aluminum would detach entirely from the thimble and fall below. The portion of the thimble opposite the point of safety rod / thimble contact would distort but not melt. In this manner the thimble would maintain some structural integrity and hence not

collapse. Furthermore, oxidized aluminum from the thimble showed a tendency to cling to the stainless steel safety rod surface.

Numerical studies were performed in support of these experiments. Two finite element models were created to model the heat conduction-radiation between the stainless steel heater and thimble. The predicted temperatures for the heater and thimble were in good agreement with the experimental results.

This report details the apparatus and instrumentation used, test procedure, data collected, and numerical studies performed. Phenomenological explanations are proposed for the experimental results.

ACKNOWLEDGEMENTS

The author would like to take this opportunity to thank the many individuals who have contributed to the success of this project. In particular: A. L. Jones and S. B. Englert who helped design, construct, and instrument the experimental apparatus; D. J. Varacalle who assisted in the design and fabrication of the heater; T. Bennett who aided in the procurement of materials; D. M. McEligot, D. C. Mecham, J. E. O'Brien, and S. L. Zeigler for their very thoughtful suggestions; and finally W. G. Lussie who conceived of and secured funding for this effort.

CONTENTS

TABLES

FIGURES

NOMENCLATURE

A	Surface area, m^2
c_p	Specific heat capacity, kJ/kg C
D	Diameter, m
F	View factor
g	Gravitational constant, kg m/s^2
h	Combined convective and radiative heat transfer coefficient, W/m^2 C
k	Thermal conductivity, W/m C
z	Height along heated length, m
Pr	Prandtl number
Q	Volumetric heat source, W/m^3
q	Heat flux, W/m^2
q'''	Volumetric heat source
r	View factor vector length, m
Ra	Rayleigh number
T	Temperature, C
x,y,z	Cartesian coordinates

Subscripts

c	Convection
eff	Effective
i,j	Indices
inc	Inconel
f	Film
o	Outer
r	Radiation
ss	Stainless steel
th	Thermal
∞	Ambient

Greek

β	Volumetric coefficient of thermal expansion, C^{-1}
δ_{ij}	Kronecker delta
ε	Emissivity
π	Pi
ρ	Density, kg/m^3
σ	Stefan-Boltzman constant, $W/m^2 K^4$
μ	Viscosity, kg/m s

SAFETY ROD / THIMBLE MELT FAILURE CHARACTERIZATION EXPERIMENTS

1. INTRODUCTION

Experiments were conducted to study the heat transfer and melt failure characteristics of a simulated SRS nuclear reactor safety rod / thimble assembly. In the SRS reactor core a portion of the gamma energy resulting from the decay of fission products is absorbed by safety rods. The normal mechanism for removal of this energy from the safety rods is by conduction and convection to the surrounding water in the moderator tank.

The experiments described herein consider the possible results of a hypothetical loss of coolant accident (LOCA) in which the water in the moderator tank drops to approximately the twenty inch level and is replaced by air at atmospheric pressure. In the absence of surrounding water, the mechanisms for removal of energy from the safety rods include natural convection to the air, thermal radiation to the thimble and nearby fuel rods, conduction at the attachment ends of the safety rod, and direct conduction to the thimble at any points of safety rod/thimble contact. Thermal radiation, conduction, and convection to the thimble will cause the thimble temperature to increase as the safety rod temperature increases, possibly to the point where the thimble material begins to melt (the melting point for Al 6063 ranges from 616 to 652 C [1]). However, as the thimble temperature rises, the thimble material will also oxidize to some degree. The melting point for aluminum oxide (Al_2O_3) is approximately 2037 C [2].

The geometry of a SRS safety rod is detailed in Figure 1. The safety rods are 2.39 cm outer diameter and are within an aluminum "thimble" of 2.74 cm inner diameter which serves as a guide tube for insertion and withdrawal of the rod. The average gap between the safety rod and the inner thimble surface is 1.78 mm when centered. Since the length of the safety rod is approximately 3.96 m, any bowing of the safety rod or thimble may cause the safety rod to contact the thimble in one or several positions along its length.

There were several objectives for these experiments. First, the experiments were to measure what safety rod temperatures are necessary for thimble failure via melting.

Second, the experiments were to characterize the typical mode of thimble failure. Thimble failure modes that have been hypothesized range from formation of droplets of aluminum to the slumping of the entire thimble into the residual water in the moderator tank. Finally, the experiments were designed to determine any dependency thimble failure may have upon thimble position relative to the safety rod. Relative positions studied included contact along a solid portion of the thimble, contact along a perforated portion of the thimble, and the axially symmetric case of no contact (i.e., the safety rod centered within the thimble).

2. DESCRIPTION OF APPARATUS

The experiment consists of a custom built, electrical heater that simulates the safety rod and several prototypical aluminum thimbles provided by the SRS. The simulated safety rod consists of six concentric layers, as depicted in Figure 2. These various layers serve to maintain electrical isolation between instrumentation and the heater, to approximate the thermal mass of the prototypical safety rod, and to allow the stainless steel outer sheath to be replaced (if necessary) while retaining the original heater.

More specifically, the inner Aremcolox ceramic core was sized such that the overall thermal mass of the heater approximated that of a SRS safety rod. The dimensions of the Aremcolox core are 1.55 cm outer diameter and 4.52 mm wall thickness. Aremcolox is a machinable ceramic that, once fired, can resist very high temperatures. The actual heater is an Inconel 600 tube, 1.91 cm outer diameter and 1.65 mm wall thickness. Inconel 600 was chosen since its electrical resistivity changes little with temperature. Alumina-titania was chosen as a material to flame spray onto the Inconel to insulate the outer stainless steel sheath from the Inconel heater electrically. However, alumina-titania does not readily spray onto Inconel. Furthermore, there was concern that the alumina-titania would not withstand the shear forces resulting from sliding the sheath on and off. For these reasons, a 0.0762 mm thick base coat of nickel-aluminum was sprayed first onto the Inconel, then a 0.254 mm layer of alumina-titania, followed by a 1.35 mm thick layer of nickel-aluminum. This last layer was polished to 0.838 mm in thickness to maximize the area of thermal contact and hence reduce the thermal resistance to the stainless steel sheath. The outermost layer of the heater is a stainless steel tube with an outer diameter of 2.39 cm and a wall thickness of 0.124 mm. This is the same outer dimension and material as the SRS safety rods. A

narrow slot was machined along the length of the tube. This slot allowed the stainless steel tube to be opened slightly and slid over the heater. Once the stainless steel sheath was in place on the heater, stainless steel straps were spot welded across the slot to clamp the sheath onto the heater.

The thimble consists of a 3.23 cm outer diameter, 0.244 cm wall thickness aluminum alloy type 6063 tube with perforations along its length. These perforations are comprised of four staggered rows of 1.27 cm diameter holes along the length of the thimble. These holes have an axial spacing of approximately 1.78 cm. The rows are positioned at 0°, 90°, 180°, and 270° along the circumference of the thimble.

The active core lengths of the prototypical safety rods and thimbles are approximately 3.96 m. As shown in Figure 3, the thimbles used in these experiments are 60.96 cm in length while the heated length of the heater is 66.04 cm and overall length is 76.2 cm. The entire heater / thimble assembly is housed inside a 1.2 x 1.2 x 1.2 m clear polycarbonate box. The box serves to eliminate any drafts from affecting the measurements while providing visual access to the experiment. A Halmar constant current power supply was used to power the heater. Dual 00-sized cables from the Halmar power supply were attached to the Inconel tube via large copper clamps. The heater is suspended by attaching the upper copper clamp and ceramic insulators to the upper frame of the box. In this way the heater is free to expand and contract.

Contact between the heater and thimble was maintained by spring-loading the thimble against the heater. A wire was passed through the top and bottom perforations opposite from the desired line of heater / thimble contact. These two wires were each passed through ceramic blocks. The ceramic blocks serve two purposes. First, they ensure electrical isolation between the thimble and the enclosure frame. Second, they can pivot and hence allow the thimble to freely expand and contract vertically. The blocks were attached to 0.635 cm diameter aluminum rods. The opposite ends of the aluminum rods pass through a frame mounted sleeve, spring, and spring clamp. The clamp was positioned on the rod such that the deflection in each spring was 1.59 mm. This corresponds to approximately 2 lb_f between the thimble and heater at top and bottom. This force was the same for the first three thimble melt experiments. To prevent the heater from bending due to the force of the spring-loaded thimble the bottom of the heater was allowed

to rest laterally against a ceramic block. In the fourth melt failure test, the heater rod was maintained centered within the thimble through the use of a series of centering screws.

3. INSTRUMENTATION

The measurements taken for these experiments included: voltage across the heater, current through the heater, stainless steel skin temperature of the heater, and thimble temperature at several positions on the thimble. Some of these time dependent measurements were recorded continuously by a data logger (discussed in Section 4) while others were recorded manually.

Heater and thimble temperatures were measured with standard grade Chromel-Alumel (type K) 0.254 mm thermocouples. The heater thermocouples were attached to the stainless steel heater surface by spot welding each thermocouple lead separately, forming an intrinsic junction on the heater surface. The rear (opposite the area of contact between the heater and thimble) heater thermocouples were strain-relieved by spot welding a strap to the stainless steel across the insulated thermocouple leads. The thimble thermocouples were made by first forming a 0.036" diameter ball junction at the end of each thermocouple. Then, 0.040" diameter by 0.040" deep holes were precision milled in the thimble from the outside at the desired mounting position. The ball junction was placed in the hole and the surrounding aluminum material peened against the junction, hence clamping the ball junction in the thimble.

There were essentially five series of tests. The first series involved only the heater while the last four series involved the heater and thimble. The instrumentation and measurement locations varied with each series of tests. There were two reasons for this. First, it was initially not known how the thimble would behave when melting. Second, the initial proposed scope of the project in terms of instrumentation was expanded during the course of the effort. Figures 4, 5, 6, 7, and 8 depict the measurement locations and relative orientation of the heater and thimble for each series of tests. Measurement location nomenclature is typically of the form "X#,θ" where X represents the type of temperature measurement (heater or thimble), # represents the axial location of the measurement (1 =

15.72 cm above the heater/thimble vertical centerplane, 2 = 5.24 cm above the heater/thimble vertical centerplane, 3 = 5.24 cm below the centerplane, and 4 = 15.72 cm below the centerplane), and θ represents the circumferentail location of the measurement in degrees displacement from the line of heater/thimble contact. In the case of no contact, θ represents the circumferential location in degrees displacement from the point opposite the slot in the heater sheath.

The instrumentation used for each test is listed in Table 1. Figures 4 through 8 are intended to assist in understanding the table.

4. DATA ACQUISITION AND VIDEOGRAPHY

Most of the measurements listed above were recorded by an Omega OM-272 precision datalogger. This datalogger was connected to an IBM XT computer system via RS-232C protocol. Measurements were updated on the IBM monitor every two seconds and recorded on the computer's hard disk every 15 seconds. The computer program for communicating with the datalogger and storing the data was written in IBM BASIC.

Two video cameras were utilized to monitor and to record the tests involving actual melts. Figure 9 depicts the relative locations of the cameras to the test setup. Both cameras were Sony model CCD-V801 video Hi8 8mm cameras. These cameras feature high resolution of 400 horizontal lines, stereo sound, automatic focus and exposure, and 10:1 power zoom. One of the cameras also featured a wide angle lens. This camera was mounted on a remote controlled pan/tilt device. Since the original emphasis of these test was upon visual observation, great care was taken to produce a video product that accurately represented the tests. Once the videos had been made they were edited using a Sony RME700 professional video editing system, color corrected using a Sony XV-C900 video multi color corrector, and recorded onto VHS format using a Sony SLV-R5 super VHS video cassette recorder.

5. TEST PROCEDURE

The conduct of each test followed a written procedure, included below.

1. Rope off test area and erect all necessary warning signs.
2. Turn on warning beacon and trigger warning horn to alert all personnel.
3. Turn on computer and other associated equipment.
4. Turn on and set to pause the video cameras, if they are to be used. Synchronize computer clock, datalogger clock, and video camera clocks.
5. Turn on video lighting.
6. Turn on main power disconnect to the Halmar power supply.
7. Turn on second power disconnect to the Halmar power supply.
8. Ensure that the current control potentiometer on the Halmar remote control panel is set to zero.
10. Start recording data on computer and start video recording.
11. Turn on the Halmar power supply.
12. Adjust current delivered to heater from zero to the desired final value.
13. Maintain constant current delivery by adjustment of potentiometer.
14. Periodically record the manual measurements.
15. Upon conclusion of test, adjust heater power to zero and turn off the Halmar power supply.
16. Turn off second and main power disconnects to the Halmar power supply.
17. Turn off video cameras and video lighting.
18. Turn off computer and other equipment.
19. Once the apparatus has cooled sufficiently, turn off warning beacon.
20. Remove warning ropes from area.

6. TESTS PERFORMED

Five test series were conducted. Each test series consisted of several individual tests ranging from four for Test Series 1 to 13 for Test Series 2. The tests performed followed the test matrix presented in Table 2. A description of the objective for each of the five test series follows. The specific temperature measurements made varied slightly from test

series to test series, as explained previously, but was the same for all tests within a test series.

The objective of Test Series 1 was to characterize the performance of the heater design and work out any problems in the measurement techniques or data acquisition system. The automated sampling rate for this test series was one scan of all measurement channels per minute. This scan rate was increased for subsequent test series to one scan per 15 seconds. Measurements for this test series included four heater surface temperatures, heater voltage and current, ambient temperature, and the polycarbonate box inner surface temperature in two locations.

Test Series 2 included a thimble in contact with the heater. The line of thimble / heater contact was along a solid (i.e., non-perforated) portion of the thimble. Thirteen individual tests were performed, including one melt failure test. These tests were designed to study the temperature response characteristics of the thimble with this contact orientation relative to the safety rod for various safety rod power levels. The initial tests allowed extrapolation of the power level required for melting of the thimble. The power levels of the heater were gradually increased to 95% of this estimated power level. The final melt test was conducted at 105% of the estimated required power level, which yielded a transient up to the melting temperature. Measurements included 8 thimble temperatures, 4 heater temperatures, heater voltage and current, ambient temperature, and the polycarbonate box surface temperature in two locations.

The objective of Test Series 3 was similar to that of Test Series 2. The contact orientation, however, was along a line of thimble perforations to study any effect thimble rotational orientation may have. Also, the method of supporting the thimble against the heater was modified. Instead of passing a wire through aluminum tabs welded to the thimble the tabs were eliminated and the wire was passed directly through adjacent perforations in the thimble. This modification eliminated the failure of the tab welds at high temperatures observed during Test Series 2. Eight tests were performed, again gradually increasing the heater power until melting. Measurements were also similar, although the eight thimble thermocouples were in slightly different locations.

One observation made during the second and third series of tests was a very large

temperature difference (> 200 C) from the heater to the thimble at the higher temperatures. In these tests the heater thermocouples were mounted on the heater surface 180° opposite the contact area. Thus an unknown fraction of this temperature variation was across the heater and the remainder was due to thermal contact resistance between the heater and thimble. Test Series 4 was conducted where two heater thermocouples were mounted as close to the line of heater / thimble contact as possible. Also, four thermocouples were mounted on the thimble 180° opposite from the line of contact. In this way temperature variations around the heater and thimble were determined.

The final or fifth series of tests involved a centered heater / thimble orientation. The objective of Test Series 5 was to determine the heater power level necessary to melt a non-contacting thimble. The measurements made were basically the same as for Test Series 4.

7. RESULTS

Various temperature measurements were made during all 37 tests. However, it should be emphasized that the primary product of this effort was intended to be a composite video tape of the various melt failure tests. The experimental apparatus and measurement system was not designed for a precise, quantitative heat transfer study. Furthermore, the emissivities of the safety rod and thimble used in these tests probably differ from the actual reactor safety rods and thimbles and hence the various temperatures for a given power level will differ. This should be kept in the mind of the reader during the following discussion of the measurement results.

Table 3 presents a summary of the steady state voltage, current, and temperature measurements for the 37 tests conducted. Note that for the melt tests, steady state values are replaced by the various temperatures when melting is first evident. The ensuing discussion of experimental results will describe:

- axial temperature characteristics of the safety rod
- axial temperature characteristics of the safety rod in contact with a thimble
- axial temperature characteristics of the thimble while in contact with the safety rod

- azimuthal temperature variations of the safety rod and thimble
- melt failure test results
- steady state temperature difference from the safety rod to the thimble
- power characteristics of the safety rod and thimble.

7.1 Axial temperature characteristics of the safety rod

Figure 10 presents the axial temperature profile for the simulated safety rod during Test Series 1. No thimble was present during this test series. Thus, the safety rod represents a vertical heated cylinder with a length to diameter ratio of 28.7. The total electrical power input has been divided by the total heated length of the simulated safety rod (0.686 m) to yield power per unit length (Watts / m). The temperature "error" bars account for the estimated experimental uncertainty in the thermocouple, thermocouple extension, and the data logger. The axial temperature variation along the length of the simulated safety rod was less than 25 C. At the higher temperatures the temperature variation was within the estimated error of the measurements. The local Rayleigh number is defined by:

$$Ra_z = \frac{\rho^2 g \beta z^3 (T - T_\infty)}{\mu^2} \cdot Pr$$

where

ρ - air density evaluated at T_∞

g - acceleration due to gravity

β - volumetric coefficient of thermal expansion ($1 / T_\infty$)

z - height along heated length of temperature measurement location

T - steady state temperature of heater at L

T_∞ - steady state ambient enclosure air temperature

μ - air viscosity evaluated at T_∞

Pr - Prandtl number evaluated at T_∞.

The Rayleigh number varied from 1.7×10^8 for the lowest measurement location and

lowest power level to 6.7 x 10^9 for the uppermost measurement location and highest power level. The decision to evaluate the air properties at T_∞ was based upon the recommendation of Siebers, Moffat, and Schwind [1985]. Based upon this definition of the Rayleigh number, it appears that the Rayleigh numbers for the bare safety rod data span the transition region from laminar to turbulent natural convection if the safety rod is considered a flat plate with a sharp leading edge. This observation is useful for interpreting the change in temperature profile with input power. As the input power to the simulated safety rod is increased, the peak of the axial temperature profile moves down the rod. This change in temperature profile may possibly be explained by a corresponding downward movement of the transition region.

7.2 Axial temperature characteristics of the safety rod in contact with a thimble

Figures 11 through 14 are comparable plots of the axial safety rod temperature variation for the test series where a thimble was present. Again, the variation in temperature remained less than 25 C for all tests with the higher temperatures typically appearing in the lower half of the safety rod. However, no apparent trend in temperature profile is evident. If one considers the error bands in the data, the temperature profile can be considered uniform for almost all the tests. Furthermore, thermal expansion of the simulated safety rod and thimble caused physical distortions and hence whether there is a continuous line of contact between the safety rod and thimble along their lengths becomes questionable, especially at the higher temperatures.

7.3 Axial temperature characteristics of the thimble while in contact with the safety rod

Figures 15 through 18 depict the axial temperature variation for the thimble in Test Series 2 through 5. As with the safety rod, the variation in temperature remained less than 25 C for all tests. However, the higher temperatures were typically in the upper half of the thimble. Again, no apparent trend is evident in the temperature profile data and considering the error bands in the data and conceivable distortions in the line of contact between the safety rod and thimble, the temperature profile can be considered almost uniform.

7.4 Azimuthal temperature variations of the safety rod and thimble

In the later phase of testing it was decided desireable to measure the azimuthal variation of temperature of the simulated safety rod and thimble. This measurement was prompted from the observation of a very large temperature variation (up to and greater than 200 C) from the safety rod to the thimble. Furthermore, numerical studies were performed to study the heat transfer characteristics analytically. These studies are discussed in Appendix A found at the end of this report. The temperature drop between the safety rod and thimble will be discussed further later in this report. However, note that in prior tests (Test Series 2 and 3) the simulated safety rod temperatures were measured opposite from the line of contact between the safety rod and thimble. The thimble temperatures, however, were measured along the line of contact. Thus, it became of interest to determine what fraction of the safety rod / thimble temperature drop was attributable to a temperature gradient azimuthally around the safety rod.

Figures 19 and 20 depict the front-to-rear differences in temperature for different axial locations and power levels for the safety rod and thimble respectively in Test Series 5. The values are represented as the differences from the overall average for that particular power level. Superimposed upon these plots are the estimated errors in temperature measurement, shown as diverging straight lines rather than as error bars to simplify interpretation. Note that Test Series 5 was the centered safety rod / thimble configuration. Thus, in the absence of thermal distortion of the geometry one would expect no azimuthal variation of temperature. Careful inspection reveals several trends in the data. First, in general the front and rear temperature measurements parallel each other as the input power is varied. This observation is as one would expect. Second, the rear (i.e., along the slot in the stainless steel heater sheath) of the simulated safety rod is higher in temperature than the front by as much as 12 C. This rear-to-front temperature difference in the simulated safety rod is much less than the observed temperature drop from the safety rod to thimble. Third, in contrast to the simulated safety rod temperature differences, the front of the thimble is higher in temperature than the rear, in one case by as much as 48 C, although more typical values are less than 10 C. This is supported by results from Test Series 4. Figure 21 depicts the front-to-rear thimble temperature variations for Test Series 4. In this test series the thimble was in contact with the safety rod and front to rear thimble temperatures varied by 14 C or less.

After the fifth test series, the simulated safety rod was disassembled to attempt to explain the second and third points listed above. The outer nickel-aluminum coating and the inner surface of the stainless steel sheath were inspected, the nickel-aluminum with a microscope and the stainless steel sheath with a borescope. Discolorations and variations in the surfaces indicated that contact, and hence heat transfer, between the nickel-aluminum and stainless steel was best along each side of the split in the stainless steel sheath. Furthermore, the leads of the thermocouples mounted on the rear of the safety rod were routed upward parallel to and between the safety rod and thimble. This partial blockage of the safety rod / thimble gap may have influenced any natural convection occurring in the gap. These same thermocouple leads may have affected the radiative heat transfer to the thimble by acting as a radiation shield, with the result being that more heat was transferred to the front of the thimble than the rear.

7.5 Melt failure test results

Table 4 presents a summary of the melt failure test findings. The melt tests were the last tests in Test Series 2 through 5 (test numbers 2.13, 3.8, 4.5, and 5.7). Figures 22 through 25 present traces of temperature versus time for the four actual thimble melt failure tests conducted. Solid symbols on the plots represent safety rod or heater temperatures while open symbols represent thimble temperatures. Sudden catastrophic decreases in indicated transient thimble temperature values imply thermocouple detachment from the aluminum thimble. Figure 26 presents a photograph of the melted thimble resulting from the melt failure test of Test Series 3.

The power setting used for each melt was determined beforehand via extrapolation of that test series temperature versus power data. At test time equal to zero, the input power to the simulated safety rod was increased from zero to the desired extrapolated value. The time required for any softening or melting to begin was dependent upon the input power to the safety rod, as can be seen in Table 4. As the thimble approached its melting point, the aluminum would begin to soften. Since the thimble thermocouples were attached to the thimble by inserting the thermocouple junction into a hole in the thimble and peening thimble material against and over the junction, softening of the thimble material around the thermocouple would often allow the thermocouple to detach itself from the thimble. In the

first melt, this caused all but one of the thimble thermocouples to detach before any actual melting was evident. Care was taken in subsequent tests to minimize any tension in the thermocouple leads. Thus, the melt failure test in Test Series 3 and 4 retained more thimble thermocouples. In spite of this effort, unfortunately, all the thimble thermocouples in the Test Series 5 melt failure test detached from the thimble.

An unexpected problem arose in the first melt failure test (test 2.13) with the method of attachment between the thimble and the supports. Aluminum tabs had been welded to the thimble at the top and bottom. The support rods were then attached to these rods via ceramic insulating blocks. As the melting temperature was approached, the tab welds failed, allowing the thimble to slide down along the safety rod onto the lower electrical power attachment bracket and simply lean onto the safety rod.

In Test Series 3 and 4, the thimble was attached to the ceramic insulating blocks by passing stainless steel wire through a thimble perforation at the top and bottom of the thimble. With the improved method of support in Test Series 3 and 4, as the aluminum thimble would soften, the thimble would also distort. Typically, the top and bottom of the thimble would remain in contact with the safety rod while the middle of the thimble would bow away from the safety rod. Furthermore, the force imposed by the support rods to hold the thimble in contact with the safety rod would stretch the upper and lower attachment points of the thimble. Due to the improved thimble / safety rod contact at top and bottom, the top and bottom sections of the thimble were the first to show evidence of melting for the melts in Test Series 2, 3, and 4. In Test Series 5, the thimble was initially centered. However, at the higher temperatures, the thimble bowed and contacted the safety rod near the middle. Thus, in this case, melting was first observed near the middle of the thimble.

In all cases, melting only occurred where there was contact between the thimble and safety rod. The softening of the thimble improved the contact between the thimble and safety rod and allowed the thimble to act more as a extended surface, resulting in enhanced heat transfer from the safety rod to the surrounding atmosphere. This in conjunction with the heat of fusion necessary to actually melt the aluminum would lower the safety rod temperature, as can be seen in Figures 22 through 25.

Due to the high temperatures, the aluminum typically would form an oxide skin. Molten aluminum would then drain from beneath the oxide skin to a cooler section of the thimble where it would resolidify. The remaining skin would chemically attack the stainless steel of the safety rod and attach to it. The regions of resolidification as well as the remaining oxide skin can be seen in Figure 26. Some pitting of the stainless steel surface resulted from the chemical attack of the oxide upon the stainless steel. Very little aluminum, and only in two of the four melt tests, detached entirely from the thimble. The section of thimble material opposite the line of contact served as a support, preventing the thimble from collapsing. The attachment of the oxide skin to the stainless steel surface also provided some support for the thimble, although it is difficult to determine the magnitude of this additional support. A more complete understanding of the melting phenomena can be obtained from viewing the video tapes made of the four melt tests.

7.6 Steady state temperature difference from the safety rod to the thimble

The thimble material is designated as reactor grade Aluminum Alloy 6063. This particular alloy of aluminum has a melting point range of from 616 to 652 C [1]. The melt tests revealed that the thimble showed evidence of melting in the temperature range of 618 to 630 C where the temperatures are averaged along the thimble. The corresponding average safety rod temperatures ranged from 840 to 858 C. The very large temperature drop from the safety rod to the thimble was an important finding of this work. Figure 27 depicts the temperature drop from the safety rod to the thimble for different safety rod temperatures. This temperature drop can be represented as a linear function of the safety rod temperature by the equation:

$$(T_{SR} - T_T) = 0.2666\, T_{SR} - 4.17$$

where the T_{SR} represents the safety rod temperature in Celsius and T_T the thimble temperature in Celsius. In other words, the thimble averaged only 73% of the safety rod temperature rise for these tests. Note that for the centered melt, the temperature of the safety rod is only slightly higher (20 to 30 C) than for the contact melts. There was no appreciable difference between contact with a line of perforations versus contact with a solid portion of the thimble. The explanation for these observations probably resides in the degree of contact between the safety rod and thimble. Inspection of the simulated safety

rod and thimble after some of the higher temperature tests revealed that the safety rod and thimble would bow due to variations in thermal expansion. It is likely that this bowing during a test changes the thermal contact resistance by varying the amount of contact between the safety rod and thimble from a line to several point contacts. The points of contact were probably at the top and bottom thimble attachment points. In this manner, the direct thermal conduction from the safety rod to the thimble is reduced. Furthermore, this explains why most melting occurred at the top and bottom of the thimble. Utilizing many attachment points on the thimble may have alleviated this problem. However, it may be argued that the scenario of point contact between the safety rod and thimble is probably more prototypical than a long line of contact.

7.7 Power characteristics of the safety rod and thimble

The steady state temperatures of the thimble and safety rod for all tests as function of input powers are represented in Figure 28. Note that the relationship between the power requirements and thimble / safety rod temperature is that of a power law. The power per unit length required for initiating melting in the thimble is simply an extrapolation of this relationship. Finally, Figure 29 compares the power requirements for the bare safety rod with those for a safety rod within a thimble. The conclusion that can be derived from this figure is that the thimble hinders rather than augments heat transfer from the safety rod in the air environment of these experiments. This supports the previous observation that direct conduction to the thimble (i.e., any fin effect the thimble may serve) was minimal for these tests. The qualification "for these tests" is important since bowing of the safety rod and thimble reduced the contact to that resembling point contact rather than a line of direct contact. A further hindrance to heat transfer from the safety rod results from the small annular gap between the thimble and safety rod reducing the convective heat transfer compared to the case of a bare, unenclosed safety rod.

8. CONCLUSIONS AND RECOMMENDATIONS

Several important conclusions about the performance of the simulated safety rod, interactions between the thimble and safety rod, and thimble melting characteristics can be deduced from this effort. The simulated safety rod repeatedly withstood temperatures in

excess of 860 C with no noticeable degradation. Axial variations of the safety rod temperature while inside a thimble were less than 25 C for all tests and thus the temperature profile of the simulated safety rod could be considered uniform. As with the safety rod, the axial variation in temperature of the thimble also remained less than 25 C for all tests. A large temperature difference from the safety rod to the thimble was measured. At temperatures approaching the melting point of aluminum this temperature difference was in excess of 200 C. Azimuthal temperature differences in the safety rod and thimble were found to be on the order of 12 C or less. The explanation for the large safety rod / thimble temperature drop probably resides in a lessening in contact between the safety rod and thimble due to thermal distortions or "warping" of the safety rod and thimble. This warping tended to change the contact from that of a line to more that of point contact.

The actual melting characteristics of the thimble were mostly rather benign. At high temperatures, the aluminum surface would form an oxide layer. As the aluminum beneath melted, it would drain beneath the oxide layer and flow to a cooler section of the thimble where it would resolidify. The oxide skin left behind would chemically attack the stainless steel surface of the safety rod and attach to it. Very little aluminum detached from the thimble. Melting only occurred in areas of safety rod / thimble contact. Portions of the thimble opposite from the area of contact retained their integrity and served as a support, preventing thimble collapse or slumping. This is illustrated in Figure 26. The measured temperature at which the thimble melted fell within the melting range of the aluminum alloy 6063. Corresponding safety rod temperatures necessary to melt the thimble were in the range of 840 to 858 C. Power requirements for melting ranged from 1389 Watts / m to 1843 Watts / m. It is anticipated that the necessary temperatures and power requirements for thimble melt failure in an actual reactor would differ to some degree due to differing material emissivities.

In interpreting the results of these tests and applying the results to the prototype situation, several experimental limitations should be considered. First, in an actual reactor loss-of-coolant accident, a steam environment would exist around the safety rod and thimble. The presence of moisture would change the radiative and convective heat transfer characteristics between the safety rod and thimble as well as the oxidation rate of the thimble material, both of which could change the melt characteristics of the thimble. This effort used a dry air environment.

In the reactor, there is some heat generation within the thimble itself due to gamma heating of its aluminum alloy. This direct heat generation within the thimble was not simulated in these experiments. Thus, it is not known what effect this heating has upon the melting characteristics of the thimble.

Finally, due to the distortions in the simulated safety rod and thimble at elevated temperatures, a line of safety rod / thimble contact could not be maintained throughout the tests. By use of many thimble support points, it may be possible that line contact could be maintained. It is anticipated that with a line of contact the average temperature drop from the safety rod to the thimble may be significantly less than that measured in this effort.

REFERENCES

1. Reynolds Metals Co., "The Aluminum Data Book," Reynolds Metals Co., Richmond, VA, 1961.

2. Rankratz, L.B., "Thermodynamic Properties of Elements and Oxides," Bulletin 672, United States Department of the Interior, 1982.

3. Siebers, D.L., Moffat, k.F., and R.G. Schwind, "Experimental, variable properties natural convection from a large, vertical, flat surface," J. Heat Transfer, 1985, 107, pp. 124-132.

4. Engelman, M. S., 1991, "FIDAP Theoretical Manual," Version 6.0, Fluid Dynamics International, Evanston, IL.

5. Ozisik, M. N., Heat Transfer A Basic Approach, McGraw-Hill, New York, 1985.

6. O'Brien, J. E., 1991, "Emissivity Measurements in Support of Experiments on Natural Convection Between a Vertical Cylinder and a Surrounding Array", EG&G Informal Report EGG-NE-10083.

7. Holman, J. P., Heat Transfer, 5th Edition,,McGraw-Hill, New York, 1981.

8. Varacalle, D. J., Personal Communication, EG&G Idaho, 1992.

Measurement	Tests	Range / Accuracy	Recording Mode
Heater temperature (H1,180°)	All	0 - 900 °C ± 1.5%	Logger
Heater temperature (H2,180°)	All	0 - 900 °C ± 1.5%	Logger
Heater temperature (H3,180°)	All	0 - 900 °C ± 1.5%	Logger
Heater temperature (H4,180°)	All	0 - 900 °C ± 1.5%	Logger
Heater temperature (H2,0°)	5.1-5.7	0 - 900 °C ± 1.5%	Logger
Heater temperature (H3,0°)	4.1-4.5	0 - 900 °C ± 1.5%	Logger
Heater temperature (H4,0°)	4.1-5.7	0 - 900 °C ± 1.5%	Logger
Thimble temperature (T1,0°)	2.1-5.7	0 - 700 °C ± 1.5%	Logger
Thimble temperature (T2,0°)	2.1-5.7	0 - 700 °C ± 1.5%	Logger
Thimble temperature (T3,0°)	2.1-5.7	0 - 700 °C ± 1.5%	Logger
Thimble temperature (T4,0°)	2.1-5.7	0 - 700 °C ± 1.5%	Logger
Thimble temperature (T1,-90°)	2.1-3.8	0 - 700 °C ± 1.5%	Logger
Thimble temperature (T2,-90°)	3.1-3.8	0 - 700 °C ± 1.5%	Logger
Thimble temperature (T3,-90°)	3.1-3.8	0 - 700 °C ± 1.5%	Logger
Thimble temperature (T4,-90°)	2.1-3.8	0 - 700 °C ± 1.5%	Logger
Thimble temperature (T1,90°)	2.1-2.13	0 - 700 °C ± 1.5%	Logger
Thimble temperature (T4,90°)	2.1-2.13	0 - 700 °C ± 1.5%	Logger
Thimble temperature (T1,180°)	4.1-5.7	0 - 700 °C ± 1.5%	Logger
Thimble temperature (T2,180°)	4.1-5.7	0 - 700 °C ± 1.5%	Logger
Thimble temperature (T3,180°)	4.1-5.7	0 - 700 °C ± 1.5%	Logger
Thimble temperature (T4,180°)	4.1-5.7	0 - 700 °C ± 1.5%	Logger
Upper copper clamp temperature	1.1-3.8	0 - 300 °C ± 1.5%	Logger
Lower copper clamp temperature	1.1-3.8	0 - 300 °C ± 1.5%	Logger
Enclosure ambient temperature	All	0 - 100 °C ± 1.5%	Logger
Top polycarbonate temperature	All	0 - 100 °C ± 1.5%	Manual
Rear polycarbonate temperature	All	0 - 100 °C ± 1.5%	Manual
Cold junction temperature	All	0 - 100 °C ± 1.5%	Logger
Enclosure relative humidity	4.4-5.7	0 - 100% ± 5%	Manual
Heater voltage	All	0 - 5 V ± 0.1 mV	Manual
Heater current	All	0-500 A ±0.01 A	Manual

Table 1. List of measurements made.

Test #	Thimble Present	Contact Orientation	Power Level (watts/m)	Melt ? (Video ?)
1.1	No	N/A	120	No
1.2	No	N/A	478	No
1.3	No	N/A	577	No
1.4	No	N/A	1076	No
2.1	Yes	Solid	26	No
2.2	Yes	Solid	112	No
2.3	Yes	Solid	260	No
2.4	Yes	Solid	378	No
2.5	Yes	Solid	260	No
2.6	Yes	Solid	381	No
2.7	Yes	Solid	521	No
2.8	Yes	Solid	675	No
2.9	Yes	Solid	759	No
2.10	Yes	Solid	802	No
2.11	Yes	Solid	854	No
2.12	Yes	Solid	952	No
2.13	Yes	Solid	1389	Yes
3.1	Yes	Perforations	26	No
3.2	Yes	Perforations	112	No
3.3	Yes	Perforations	467	No
3.4	Yes	Perforations	467	No
3.5	Yes	Perforations	733	No
3.6	Yes	Perforations	952	No
3.7	Yes	Perforations	956	No
3.8	Yes	Perforations	1460	Yes
4.1	Yes	Perforations	484	No
4.2	Yes	Perforations	751	No
4.3	Yes	Perforations	981	No
4.4	Yes	Perforations	985	No
4.5	Yes	Perforations	1843	Yes
5.1	Yes	Centered	115	No
5.2	Yes	Centered	271	No
5.3	Yes	Centered	484	No
5.4	Yes	Centered	758	No
5.5	Yes	Centered	985	No
5.6	Yes	Centered	985	No
5.7	Yes	Centered	1623	Yes

Table 2. Matrix of tests performed.

Test	Amperage (amps)	Voltage (volts)	Watts / m	H1, 180 (C)	H2, 0 (C)	H2, 180 (C)	H3, 0 (C)	H3, 180 (C)	H4, 0 (C)	H4, 180 (C)	T1, -90 (C)	T1, 0 (C)	T1, 90 (C)	T1, 180 (C)	T2, -90 (C)	T2, 0 (C)	T2, 180 (C)	T3, -90 (C)	T3, 0 (C)	T3, 180 (C)	T4, -90 (C)	T4, 0 (C)	T4, 90 (C)	T4, 180 (C)	Box T (C)
1.1	100	0.82	120	366		370		362		350															20
1.2	200	1.64	478	561		579		589		589															29
1.3	220	1.8	577	590		597		613		619															32
1.4	300	2.46	1076	698		695		700		719															38
2.1	50	0.36	26	186		194		192		181	147	146	148			153			151		142	143	142		20
2.2	100	0.77	112	365		384		386		373	272	274	273			290			294		281	280	280		25
2.3	150	1.19	260	515		534		538		532	377	382	377			396			407		399	396	398		29
2.4	180	1.44	378	586		601		604		602	425	432	423			439			450		451	448	448		31
2.5	150	1.19	260	515		535		537		529	380	385	378			397			408		401	398	399		29
2.6	180	1.45	381	583		599		602		601	428	434	423			442			452		451	455	450		30
2.7	210	1.7	521	646		662		662		665	475	482	469			489			499		501	506	499		32
2.8	240	1.93	675	700		716		716		719	519	527	512			535			548		545	552	543		35
2.9	255	2.04	759	724		740		738		745	537	544	529			547			560		563	570	561		36
2.10	262	2.1	802	734		749		747		756	545	553	536			553			563		569	577	566		36
2.11	270	2.17	854	748		760		760		770	556	563	548			565			576		580	588	576		37
2.12	285	2.29	952	770		782		779		790	575	582	567			582			591		595	602	593		42
2.13	344	2.77	1389	844		854		849		862	620	*	614			624			*		626	*	626		32
3.1	50	0.35	26	142		148		143		149	117	119			117	117		114	117		111	112			19
3.2	100	0.77	112	383		398		378		400	303	306			308	303		300	303		287	289			22
3.3	200	1.6	467	618		661		651		665	485	491			505	493		505	510		501	506			30
3.4	200	1.6	467	638		654		642		659	488	495			503	491		499	503		496	501			29
3.5	250	2.01	733	724		737		727		743	543	552			555	558		555	561		554	564			35
3.6	285	2.29	952	774		783		776		789	579	589			584	589		586	592		589	598			39
3.7	285	2.3	956	766		773		771		779	575	587			580	583		582	587		586	595			39
3.8	350	2.86	1460	839		842		843		848	620	*			618	625		620	625		623	631			38
4.1	200	1.66	484	632		648	622	644	623	638		483		471		478	477		497	485		491		488	30
4.2	250	2.06	751	717		730	700	718	702	716		541		527		525	522		544	532		545		543	34
4.3	285	2.36	981	771		780	746	766	750	768		577		562		554	553		572	560		579		574	37
4.4	285	2.37	985	764		772	739	760	742	762		569		555		548	548		566	554		575		568	36
4.5	390	3.24	1843	810		848	*	853	*	851		*		588		*	626		626	628		617		627	44
5.1	100	0.79	115	398	404	407		411	389	393		274		273		284	284		284	255		274		269	22
5.2	150	1.24	271	564	567	572		583	558	565		385		383		401	400		410	366		399		393	27
5.3	200	1.66	484	671	669	674		687	661	672		463		460		476	475		493	445		484		478	31
5.4	250	2.08	758	758	748	757		772	744	757		533		528		542	541		559	512		555		546	37
5.5	285	2.37	985	807	787	799		816	786	800		576		571		582	579		594	547		592		583	41
5.6	285	2.37	985	795	779	787		808	777	792		573		569		580	578		593	576		591		583	41
5.7	365	3.05	1623	878	853	860		869	*	833		*		*		*	*		*	*		*		*	41

* - Thermocouple failure.

Table 3. Summary of experimental data obtained.

Test Series	Power (Watts/ m)	Contact Orientation	Time Till Loss Of First TC (min)	Time Till Evidence Of Melting (min)	Avg. Temp. Of Safety Rod At Melting (C)	Avg. Temp. Of Thimble At Melting (C)
2	1389	Solid Edge	16.67	25.00	≈852	≈622
3	1460	Perforation	22.33	23.50	≈843	≈623
4	1843	Perforation	12.25	11.15	≈840	≈618
5	1623	Centered	16.83	25.00	≈858	≈630*

* - In test 5.7, all thimble thermocouples detached from the thimble before melting was evident. This value represents the value of the last thimble thermocouple just before detachment.

Table 4. Summary of melt test results.

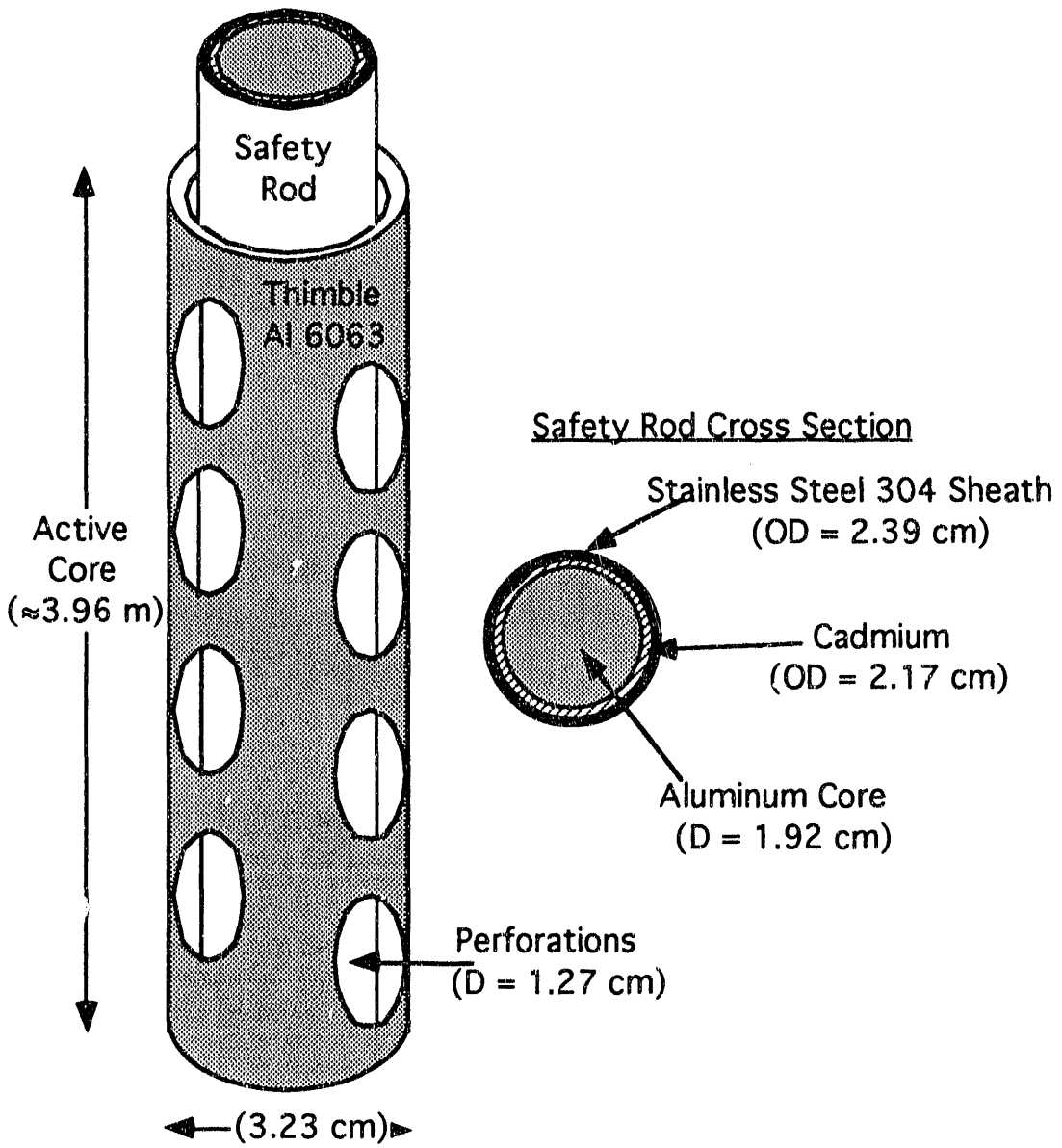

Figure 1. SRS nuclear reactor safety rod / thimble geometry.

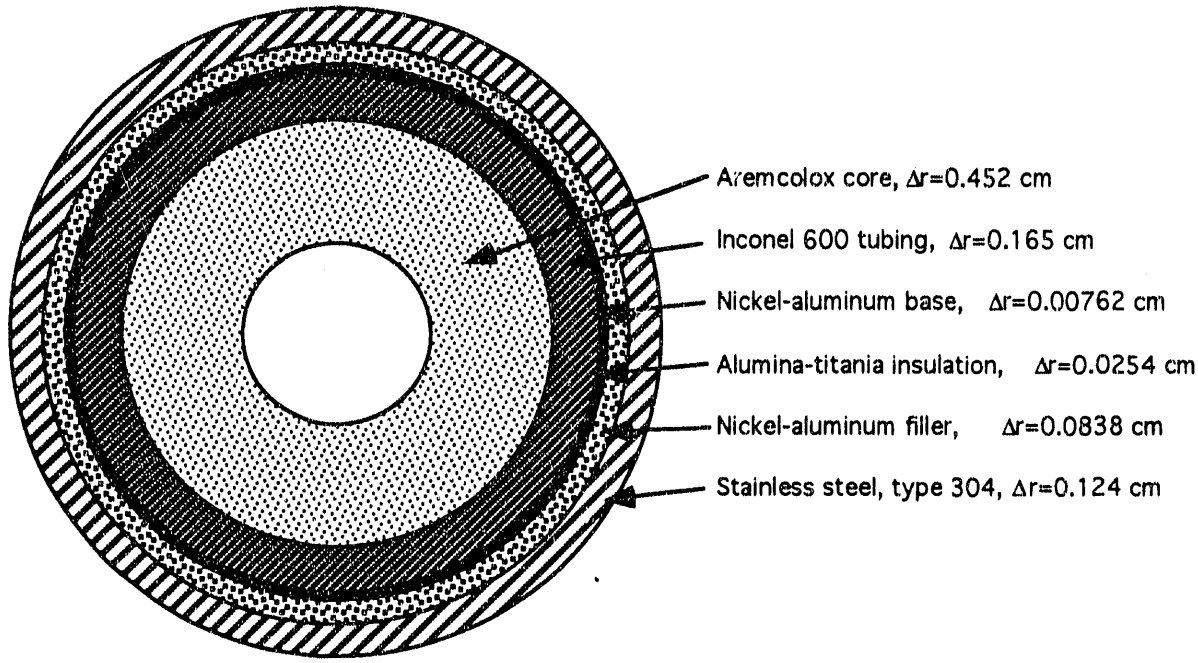

Figure 2. Electrical heater configuration to simulate the safety rod.

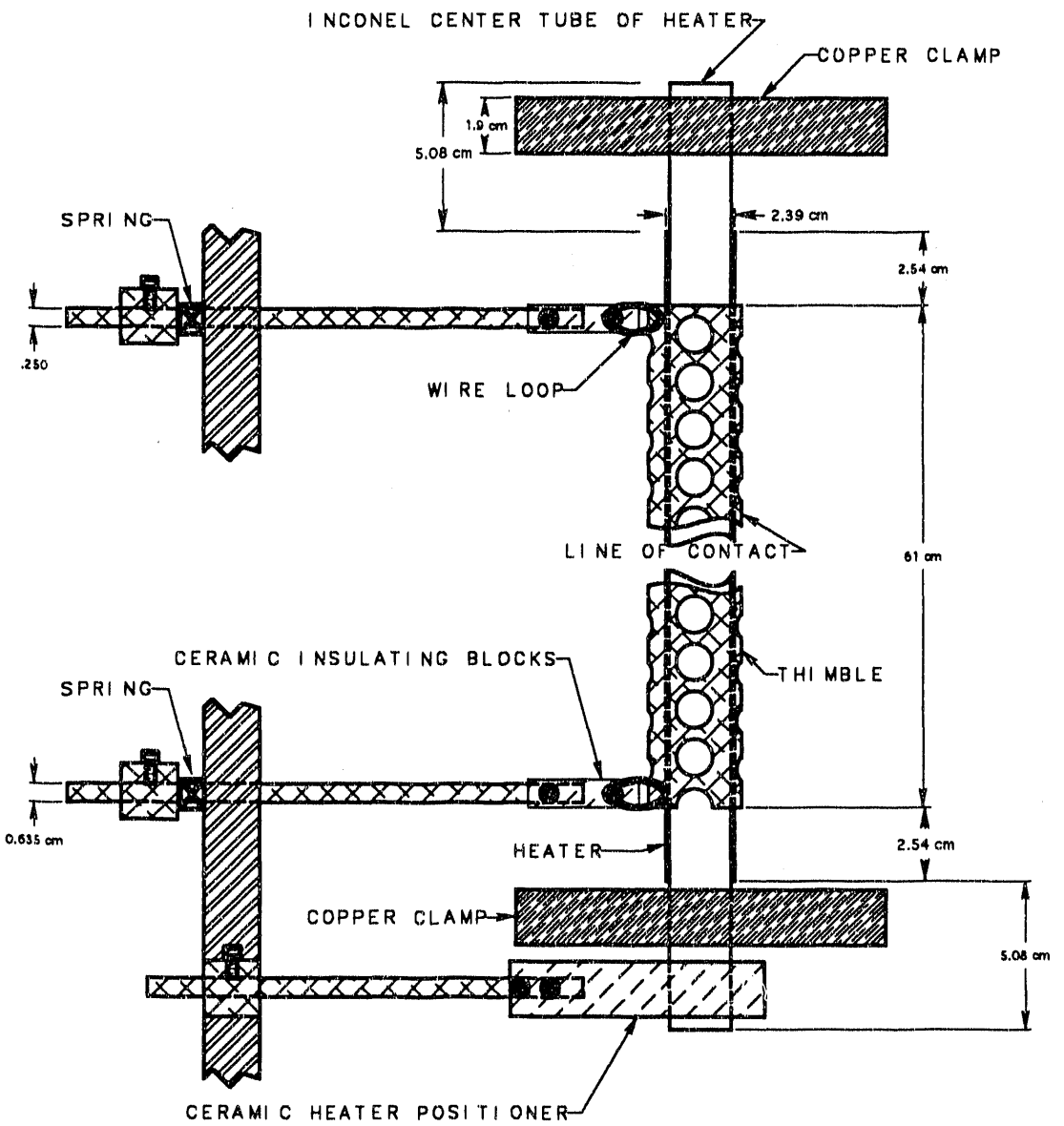

Figure 3. Experimental fixture used to maintain thimble in contact with the heater.

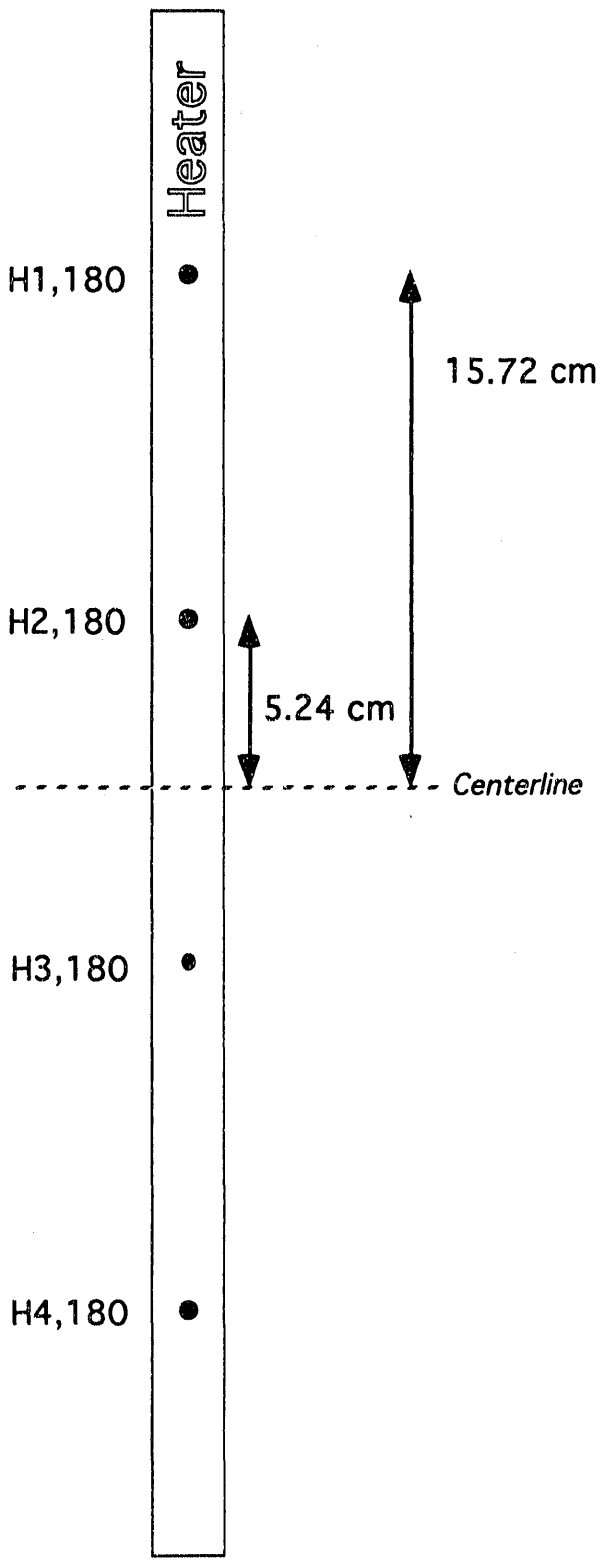

Figure 4. Temperature measurement locations for Test Series 1.

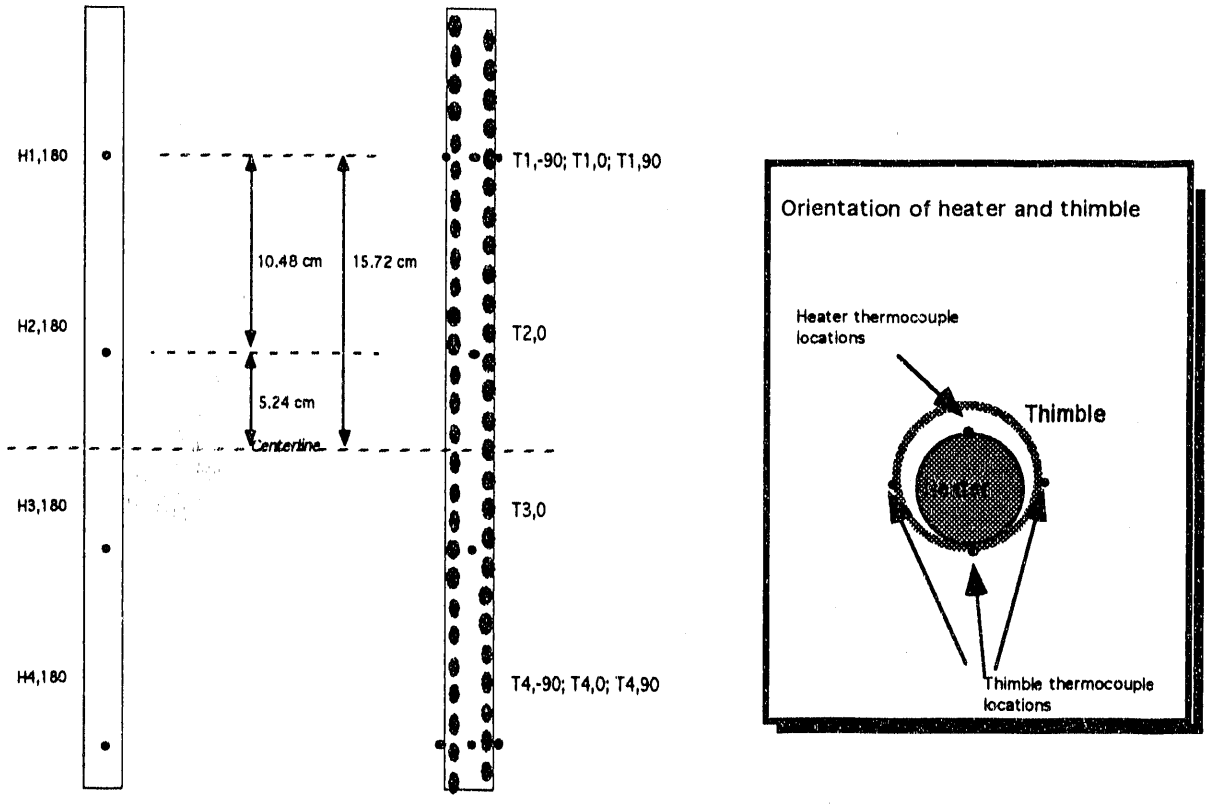

Figure 5. Temperature measurement locations for Test Series 2.

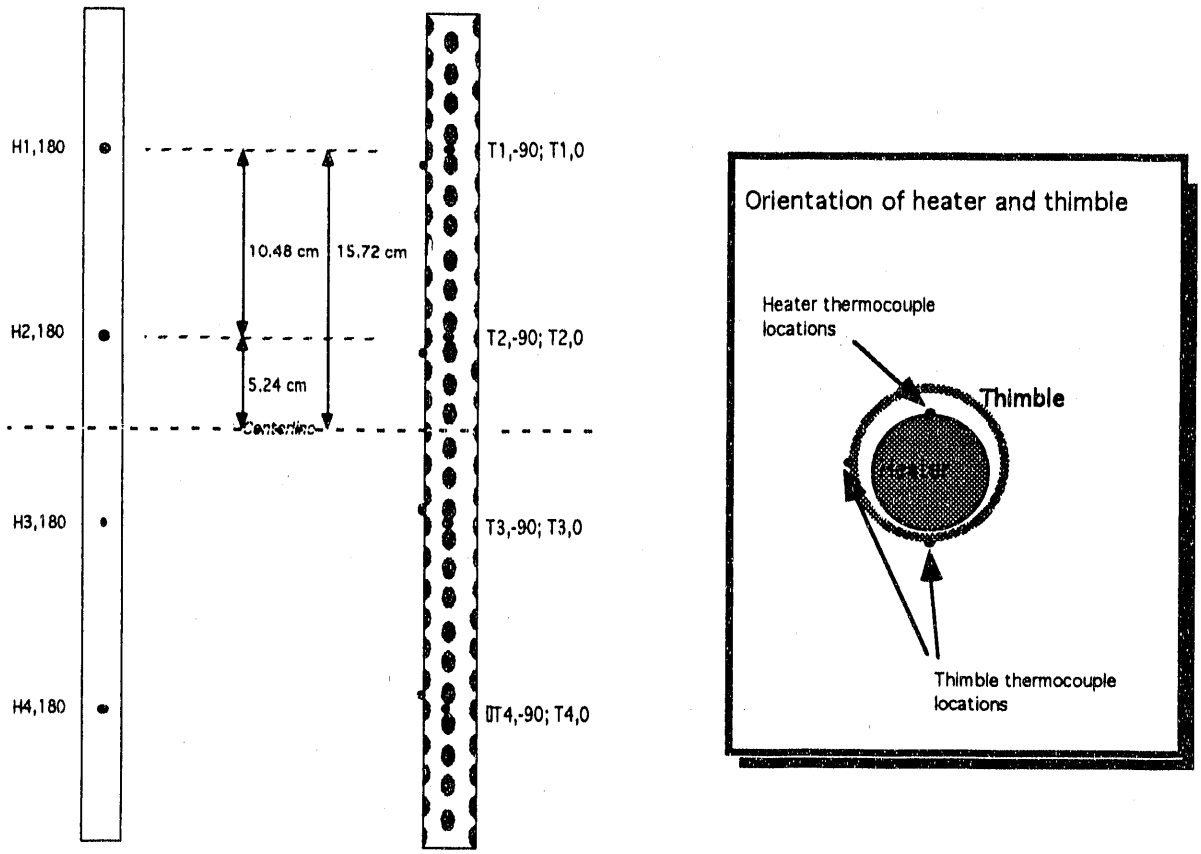

Figure 6. Temperature measurement locations for Test Series 3.

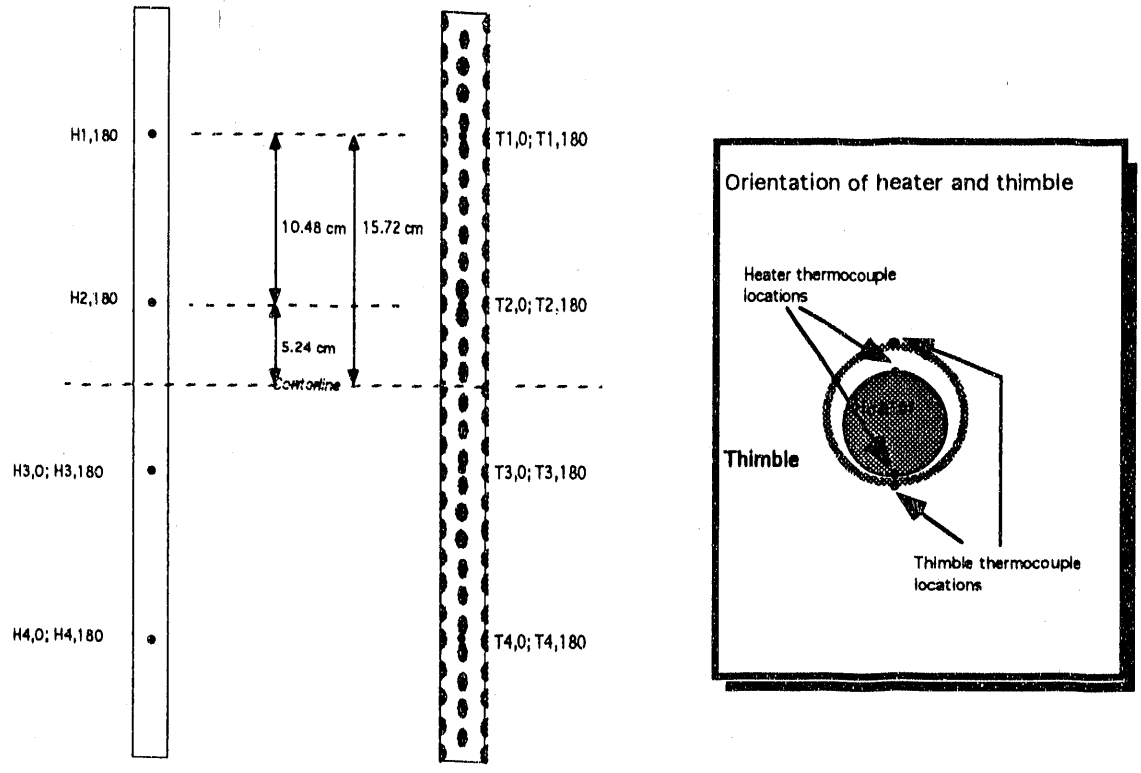

Figure 7. Temperature measurement locations for Test Series 4.

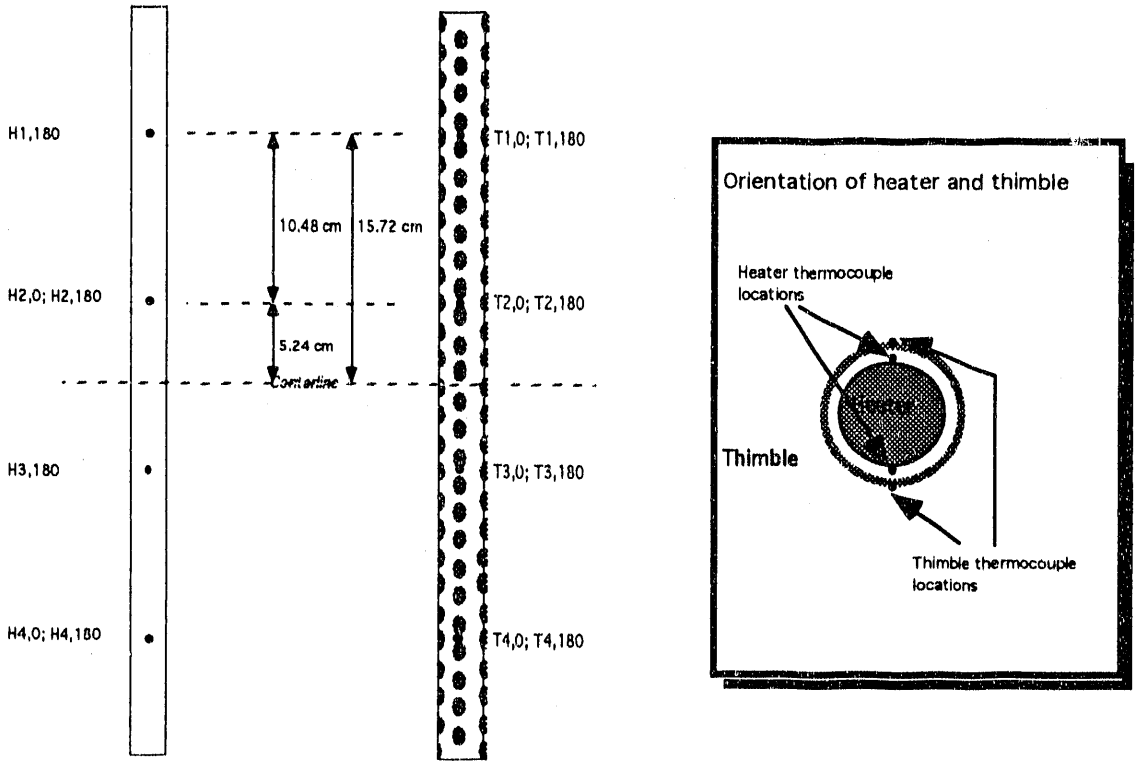

Figure 8. Temperature measurement locations for Test Series 5.

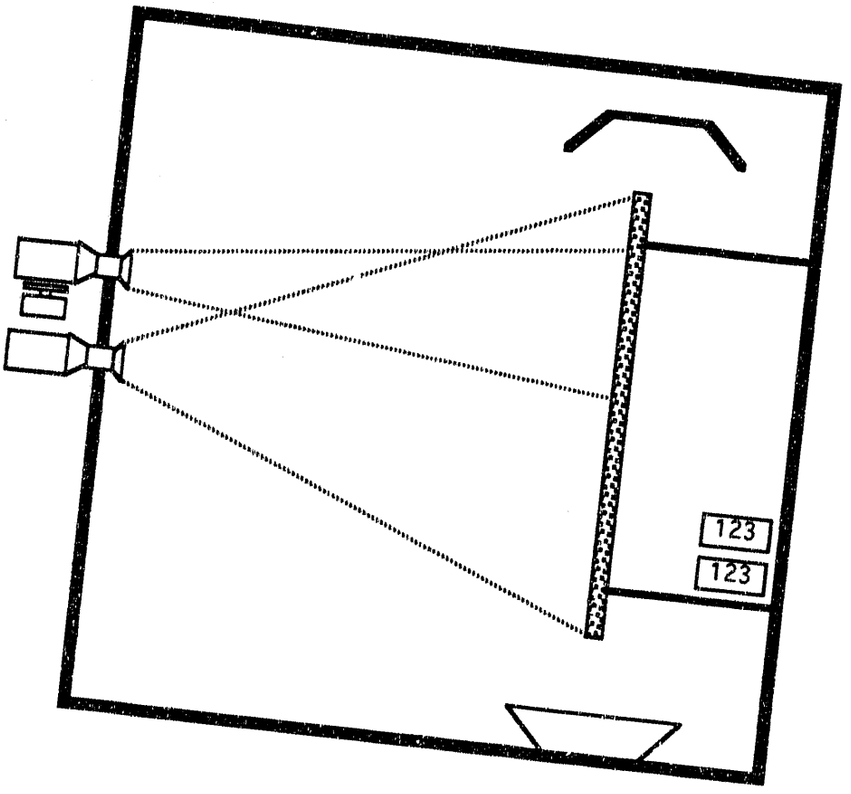

Figure 9. Location of cameras relative to the test setup.

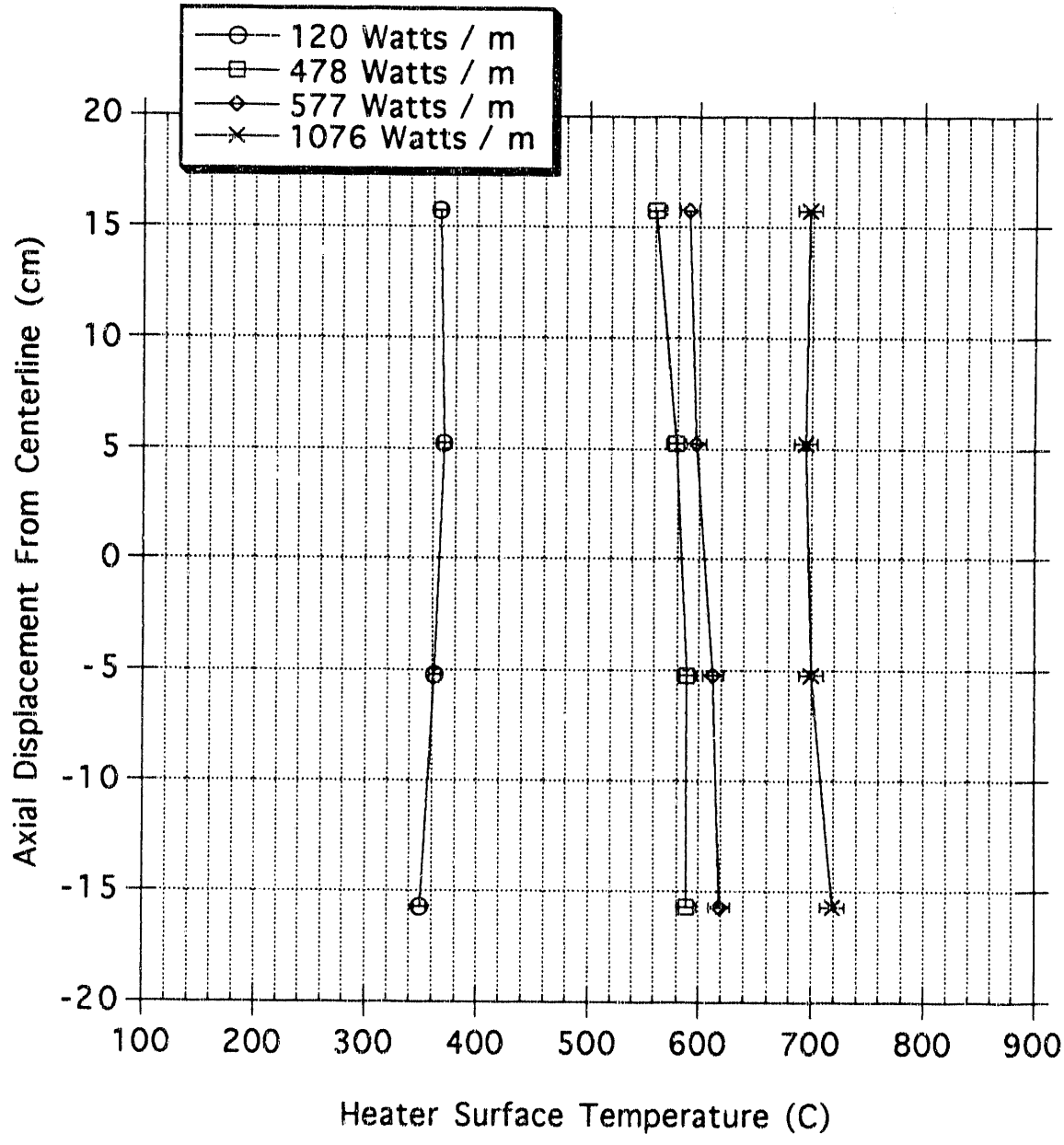

Figure 10. Heater axial temperature variation for Test Series 1 (no thimble present).

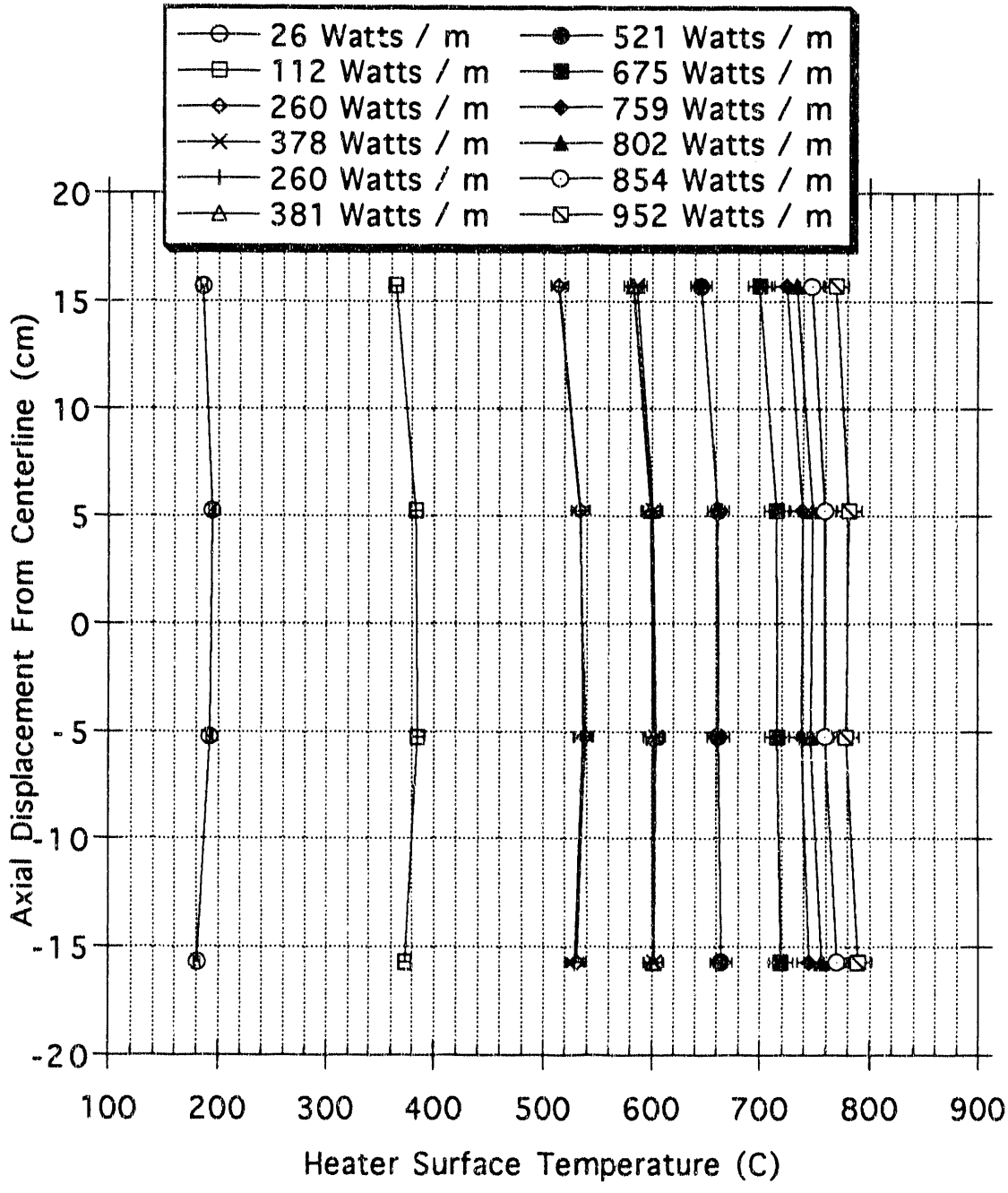

Figure 11. Heater axial temperature variation for Test Series 2.

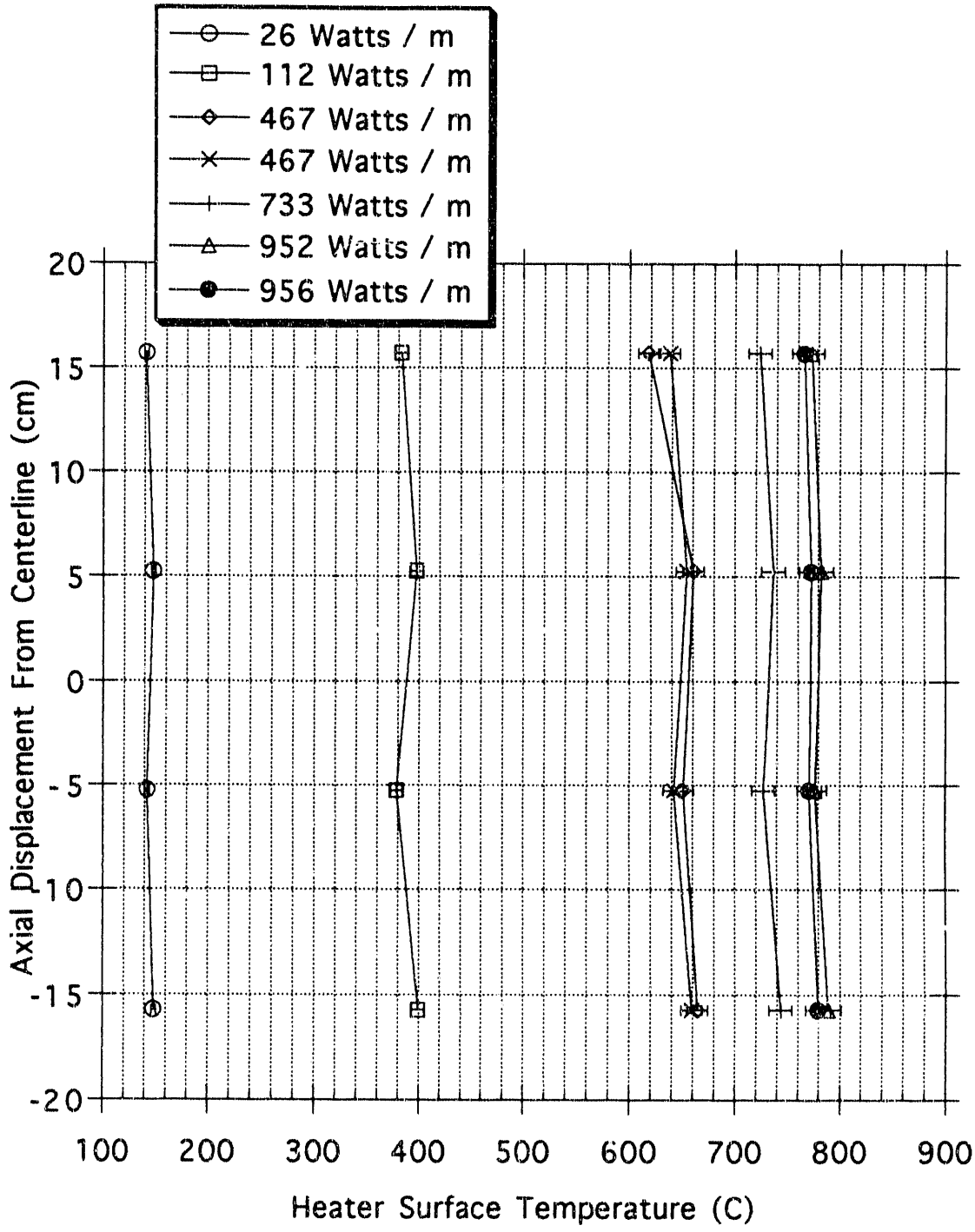

Figure 12. Heater axial temperature variation for Test Series 3.

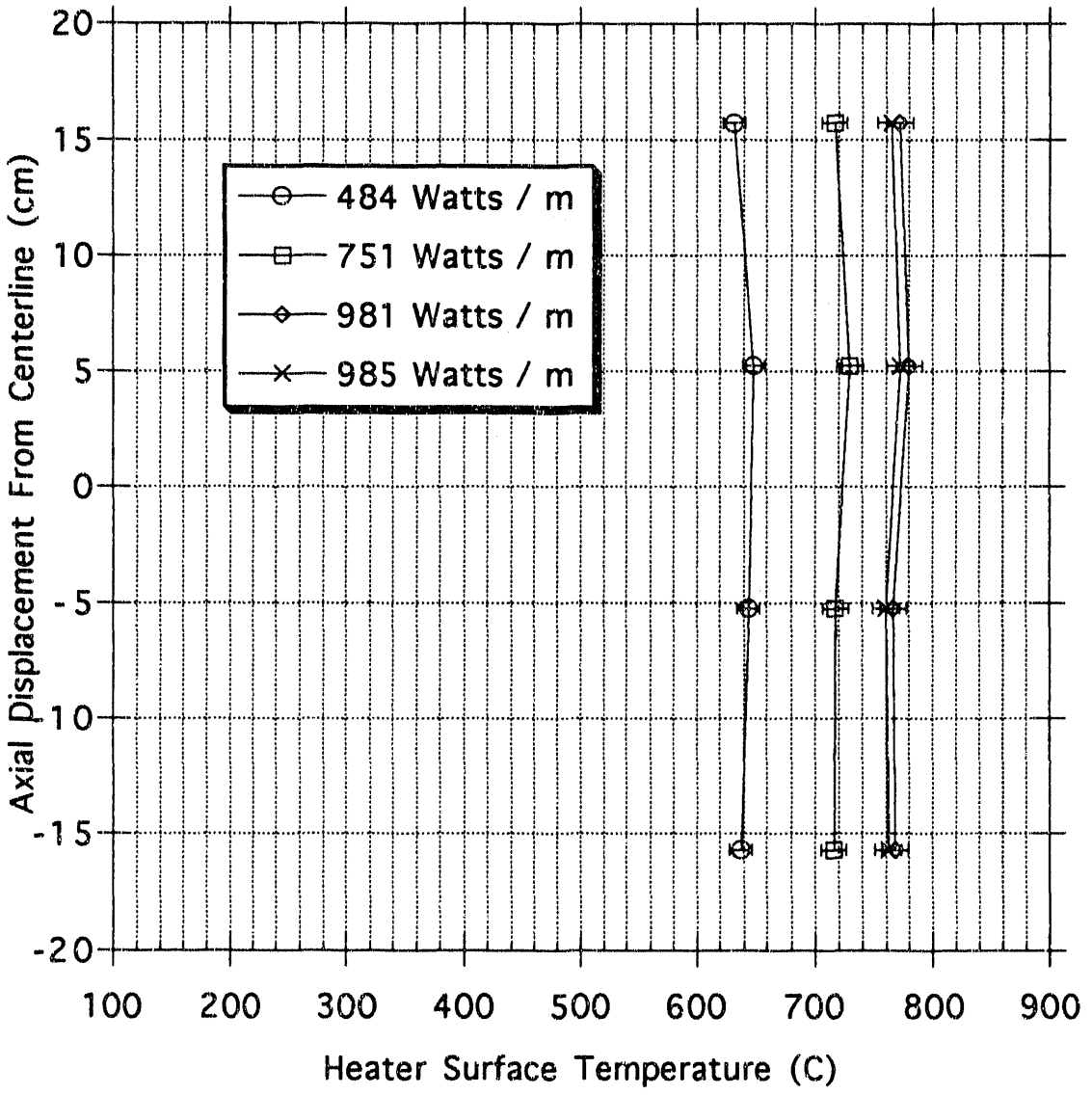

Figure 13. Heater axial temperature variation for Test Series 4.

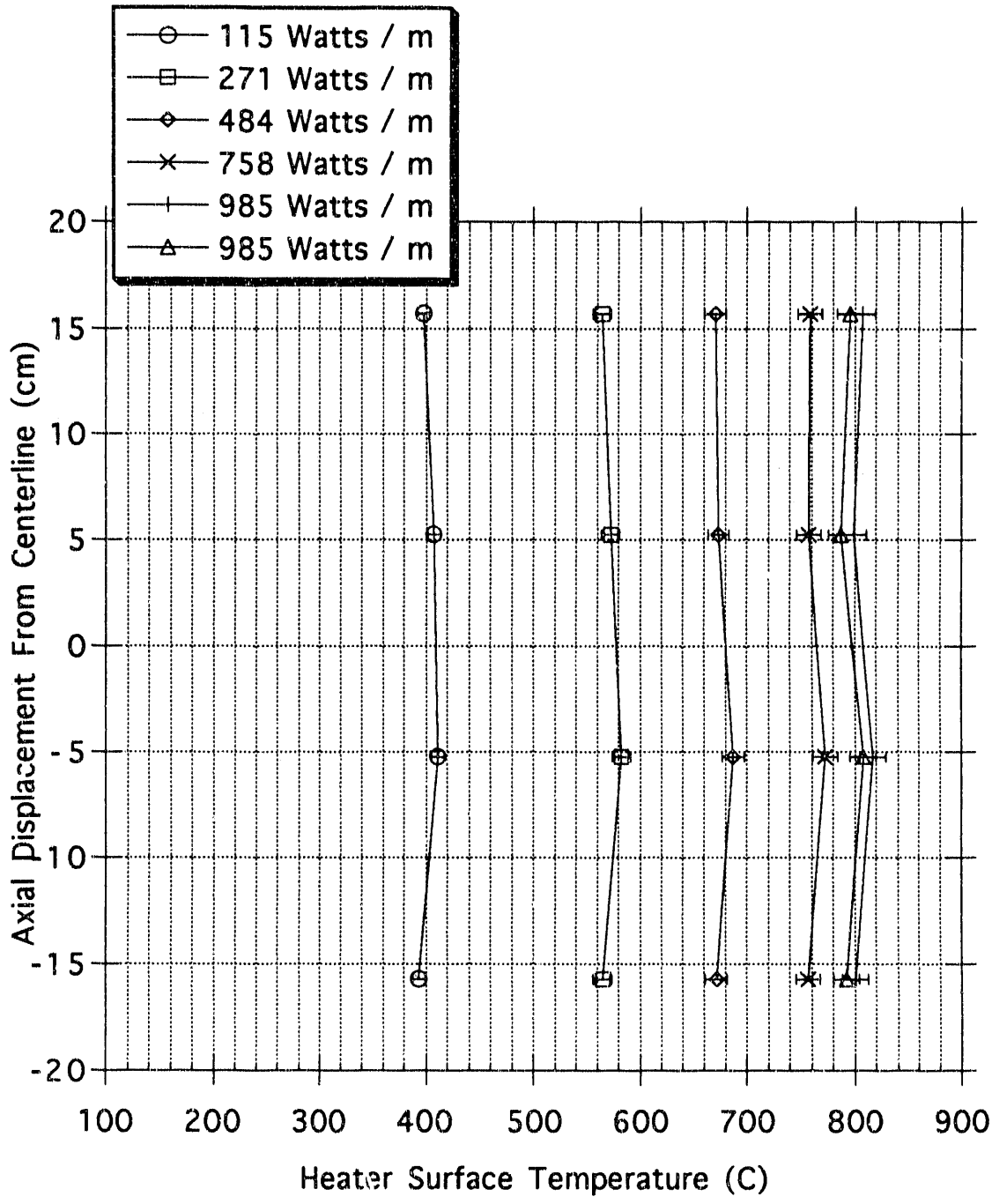

Figure 14. Heater axial temperature variation for Test Series 5.

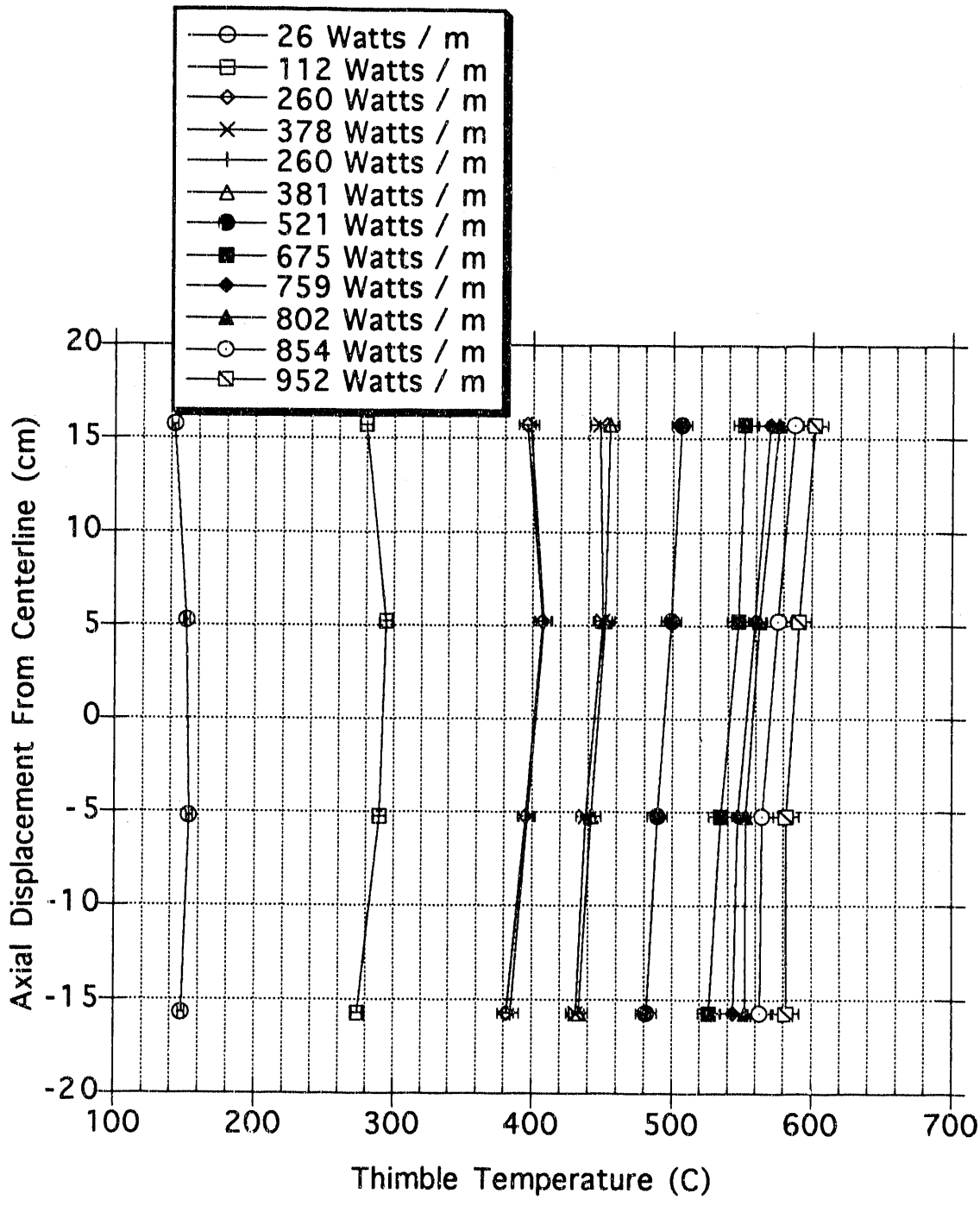

Figure 15. Thimble axial temperature variation for Test Series 2.

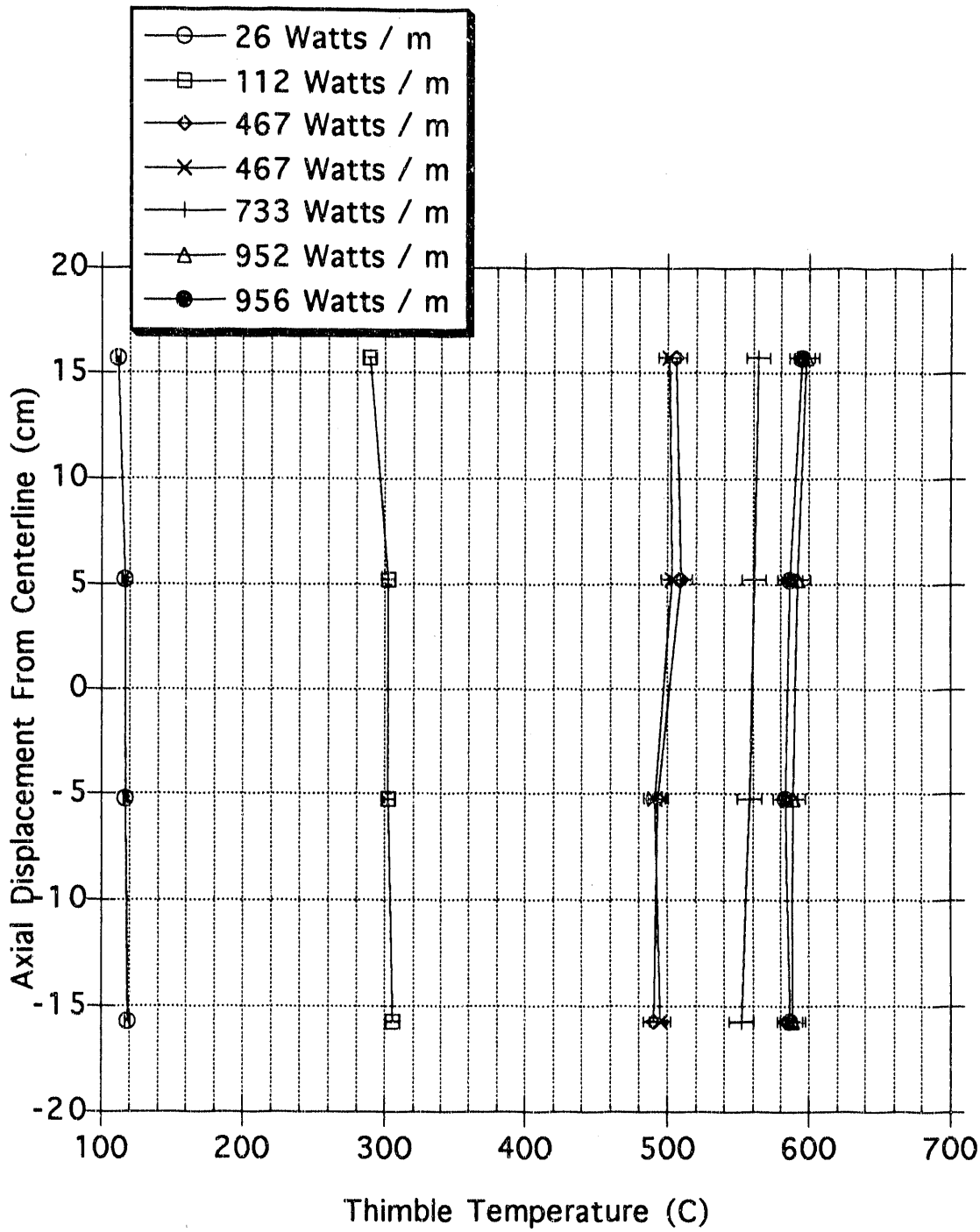

Figure 16. Thimble axial temperature variation for Test Series 3.

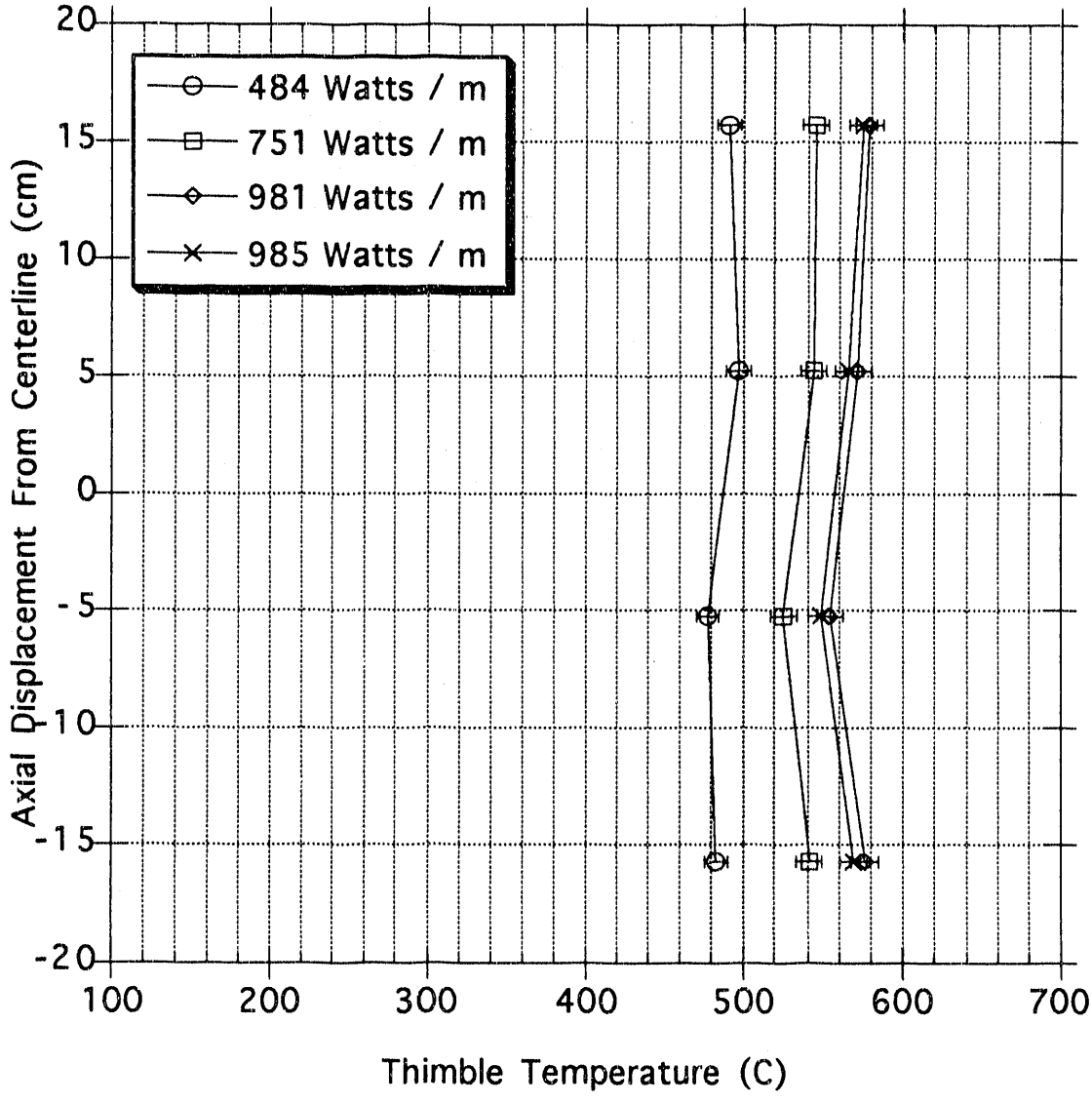

Figure 17. Thimble axial temperature variation for Test Series 4.

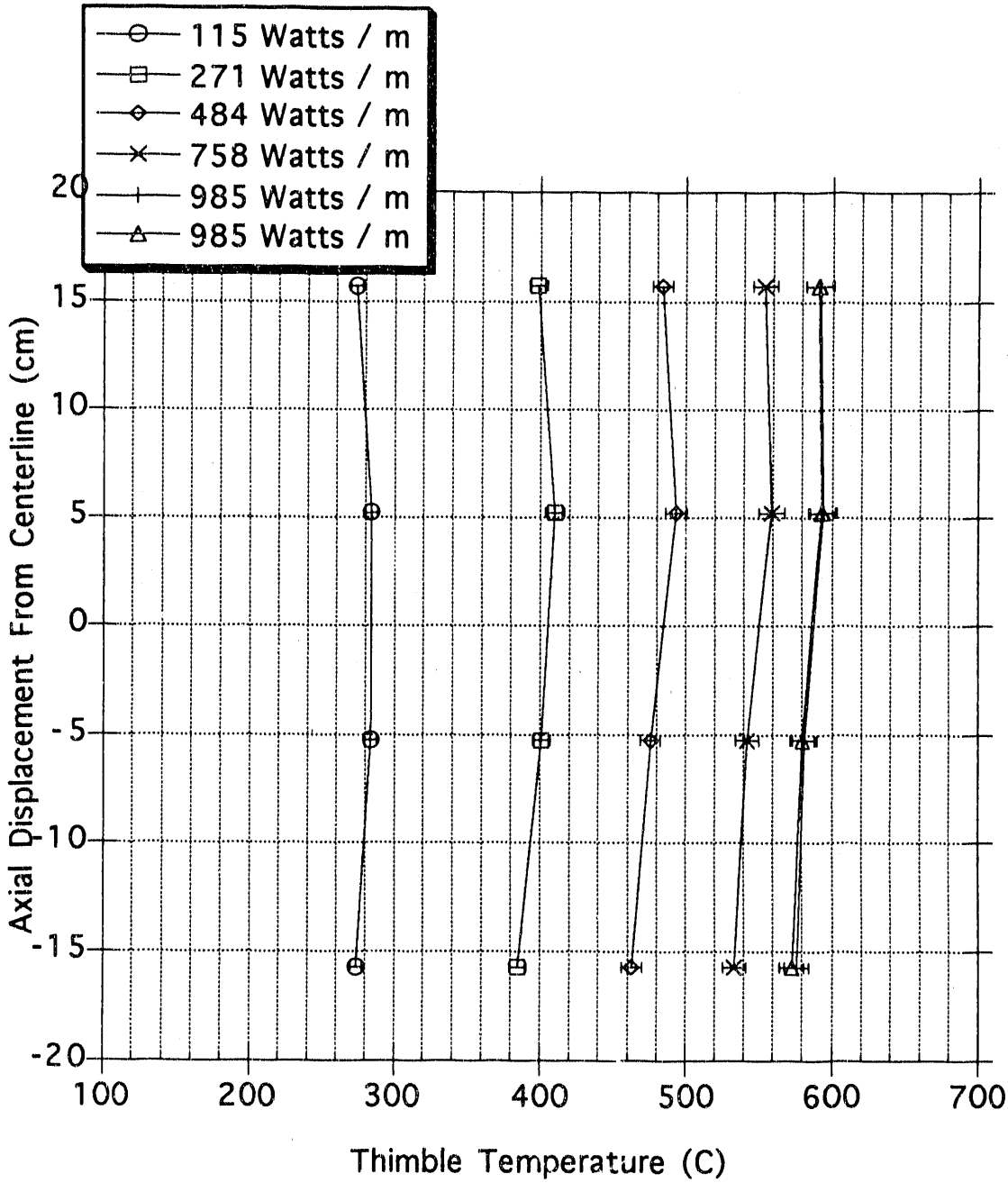

Figure 18. Thimble axial temperature variation for Test Series 5.

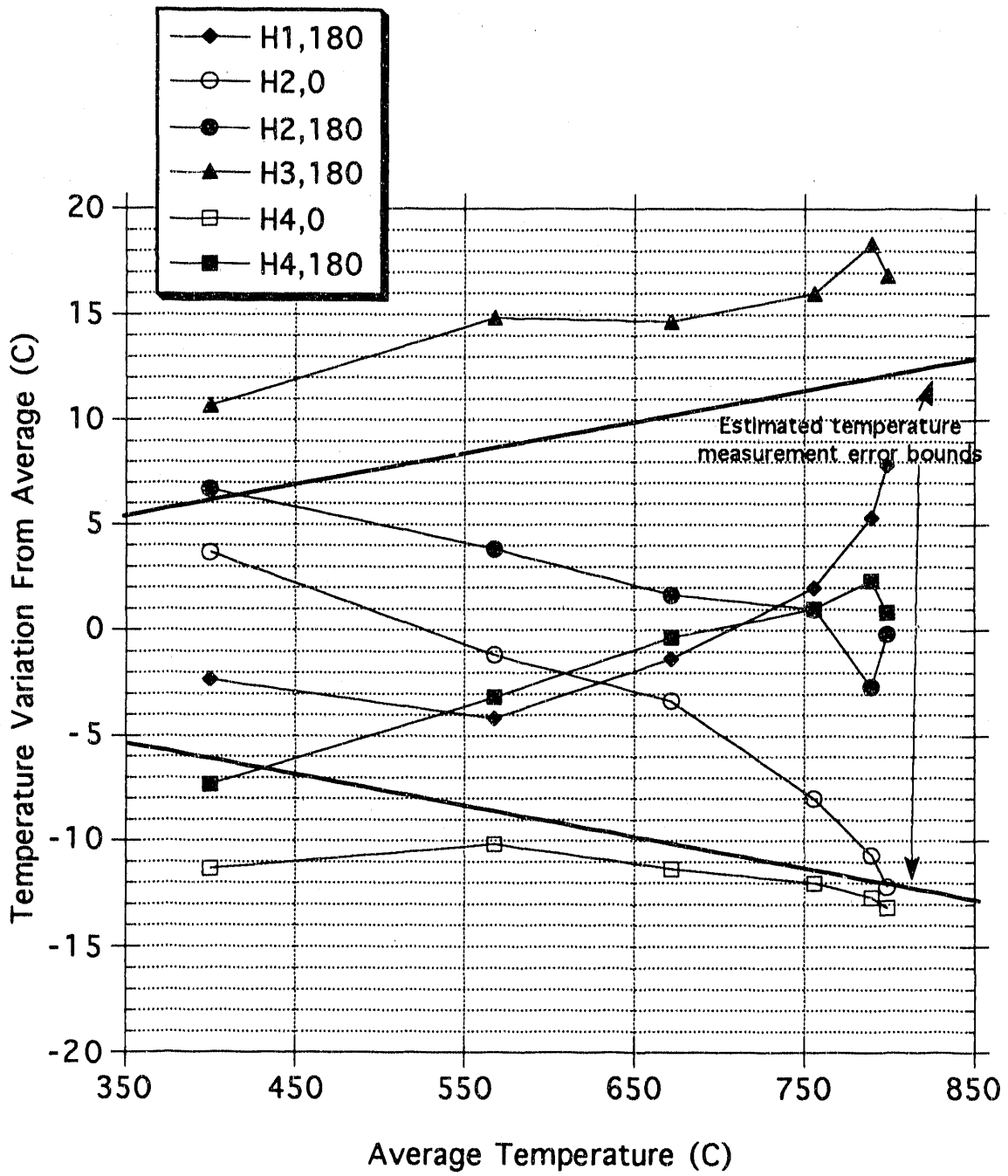

Figure 19. Heater axial and azimuthal temperature variation for Test Series 5.

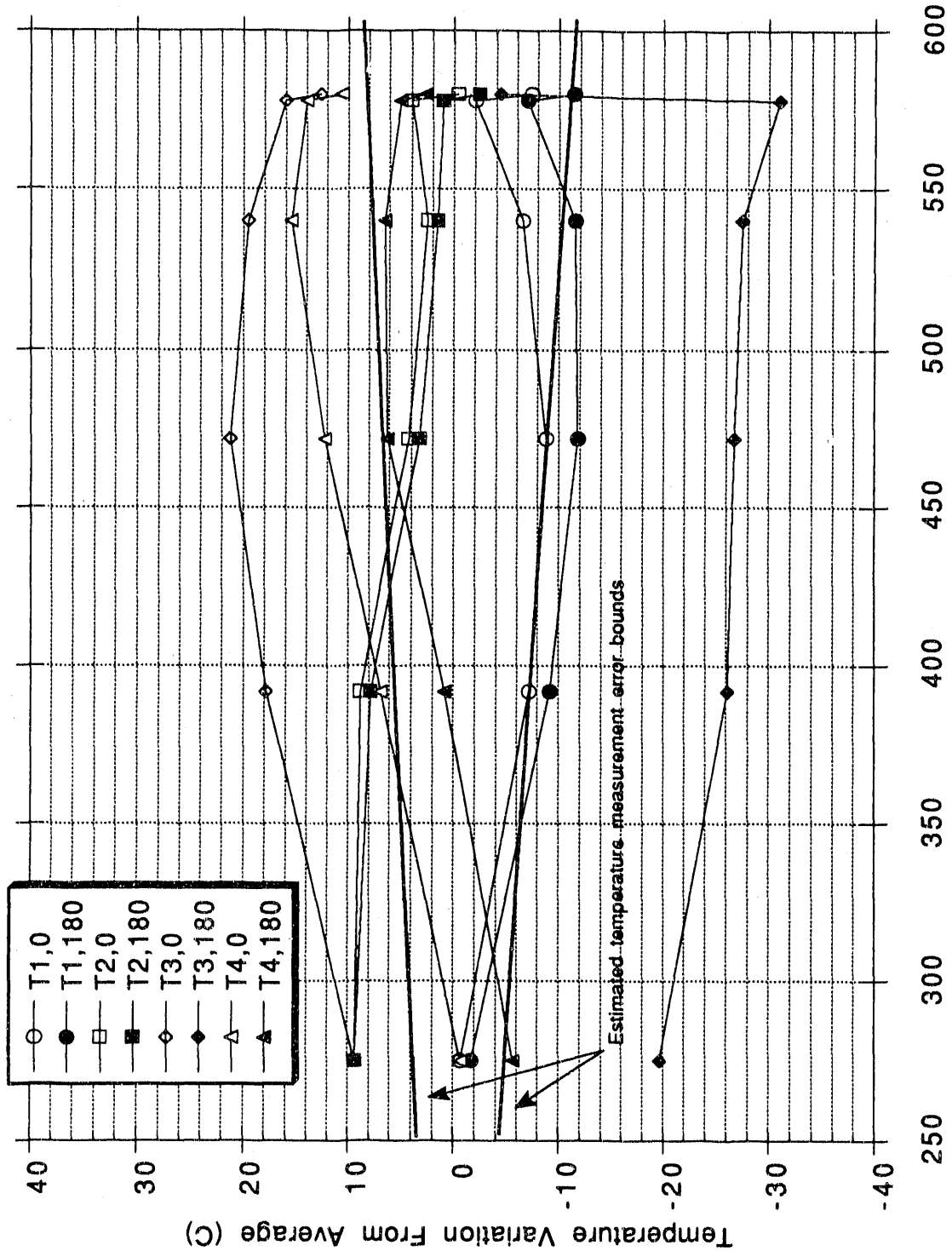

Figure 20. Thimble axial and azimuthal temperature variation for Test Series 5.

Figure 20. Thimble axial and azimuthal temperature variation for Test Series 5.

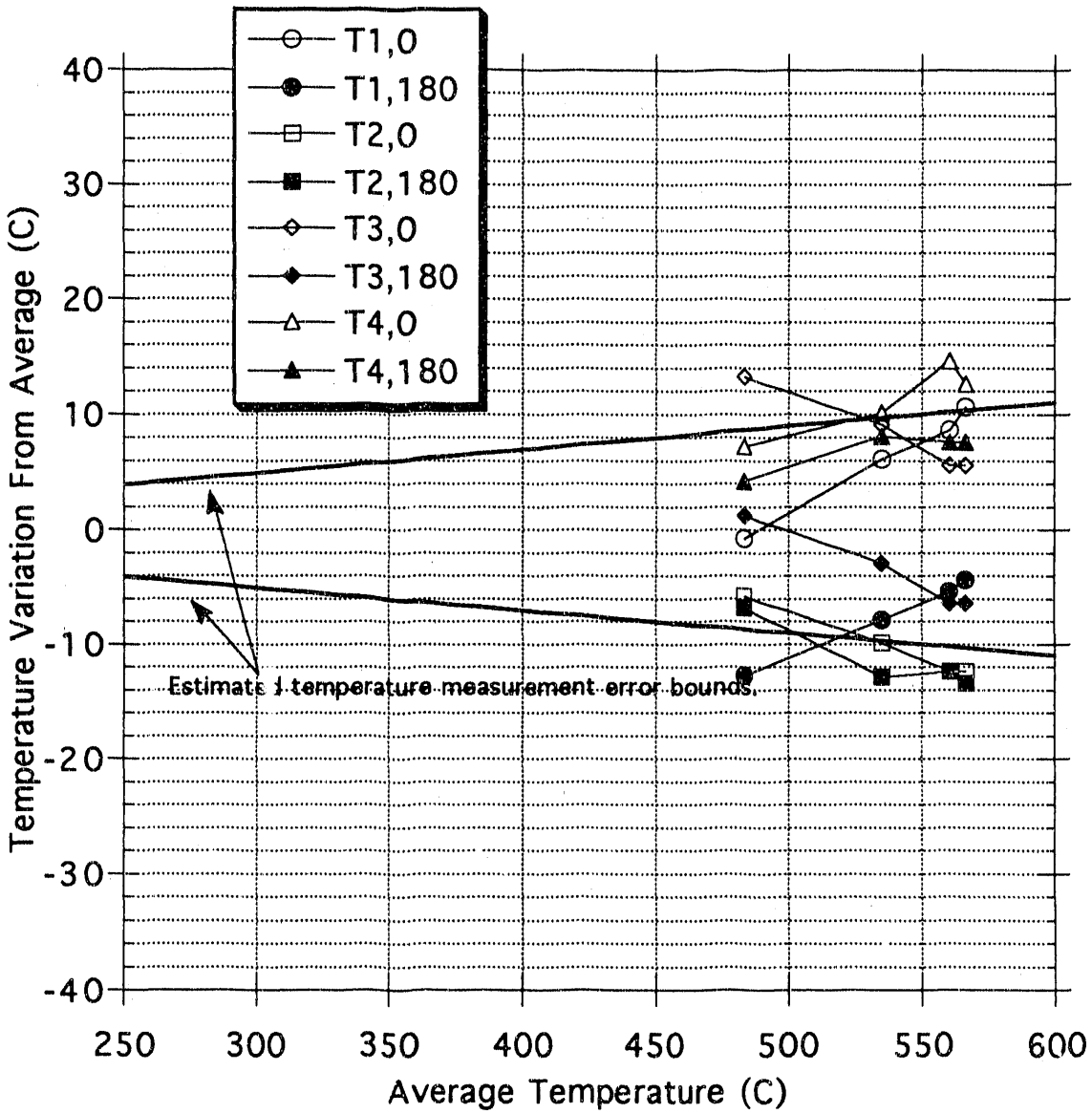

Figure 21. Thimble axial and azimuthal temperature variation for Test Series 4.

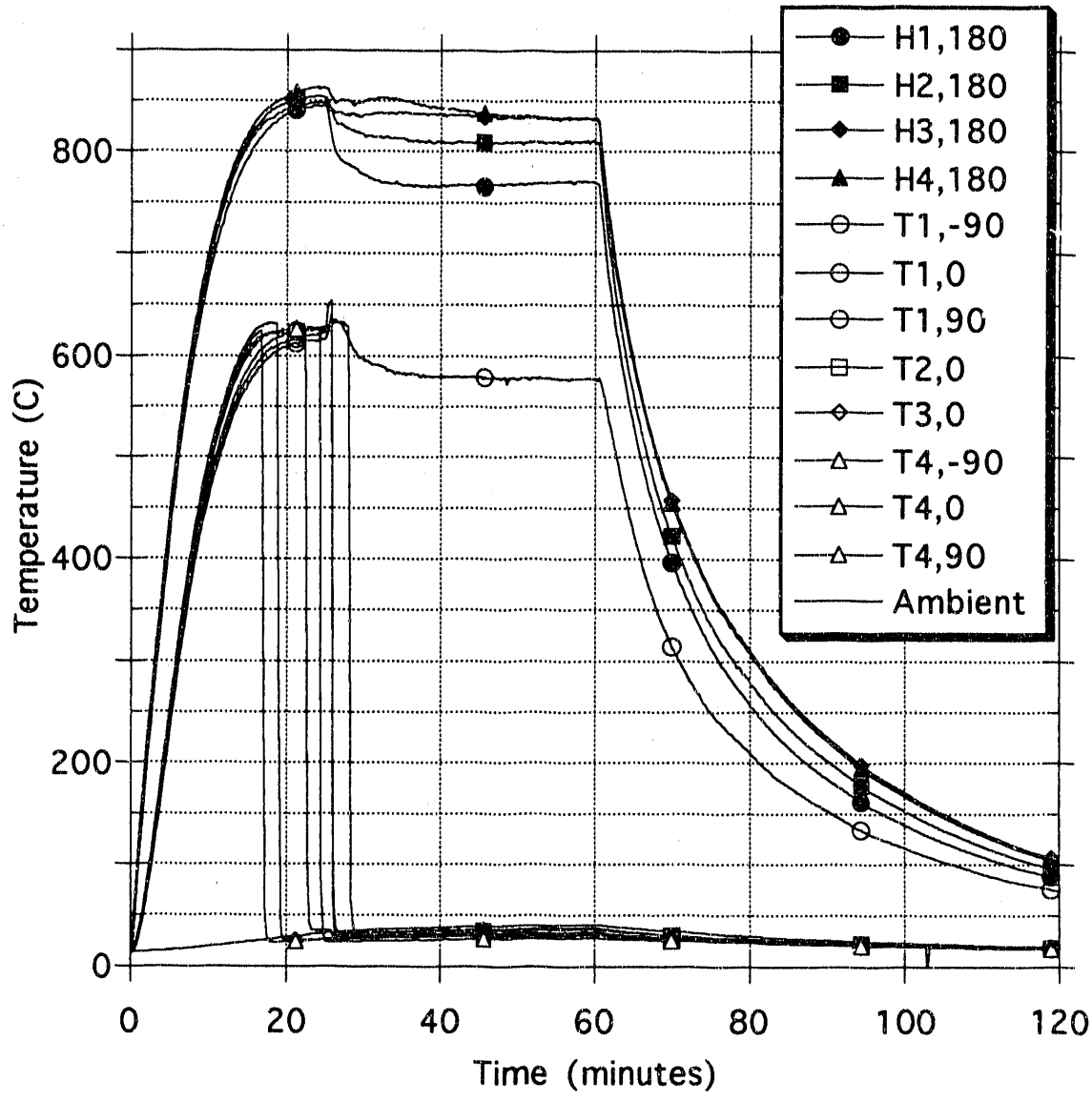

Figure 22. Heater and thimble temperatures for melt test of Test Series 2.

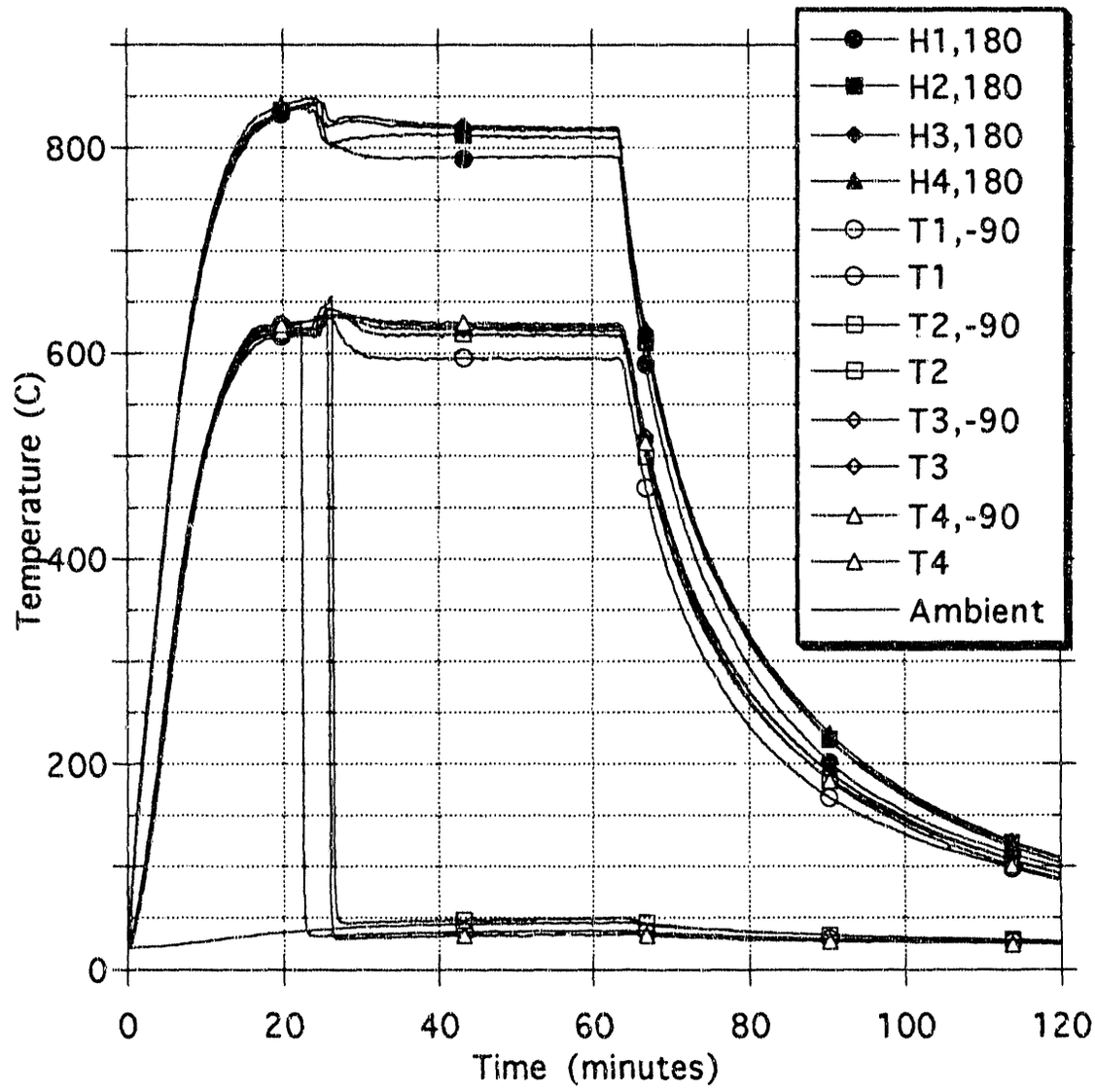

Figure 23. Heater and thimble temperatures for melt test of Test Series 3.

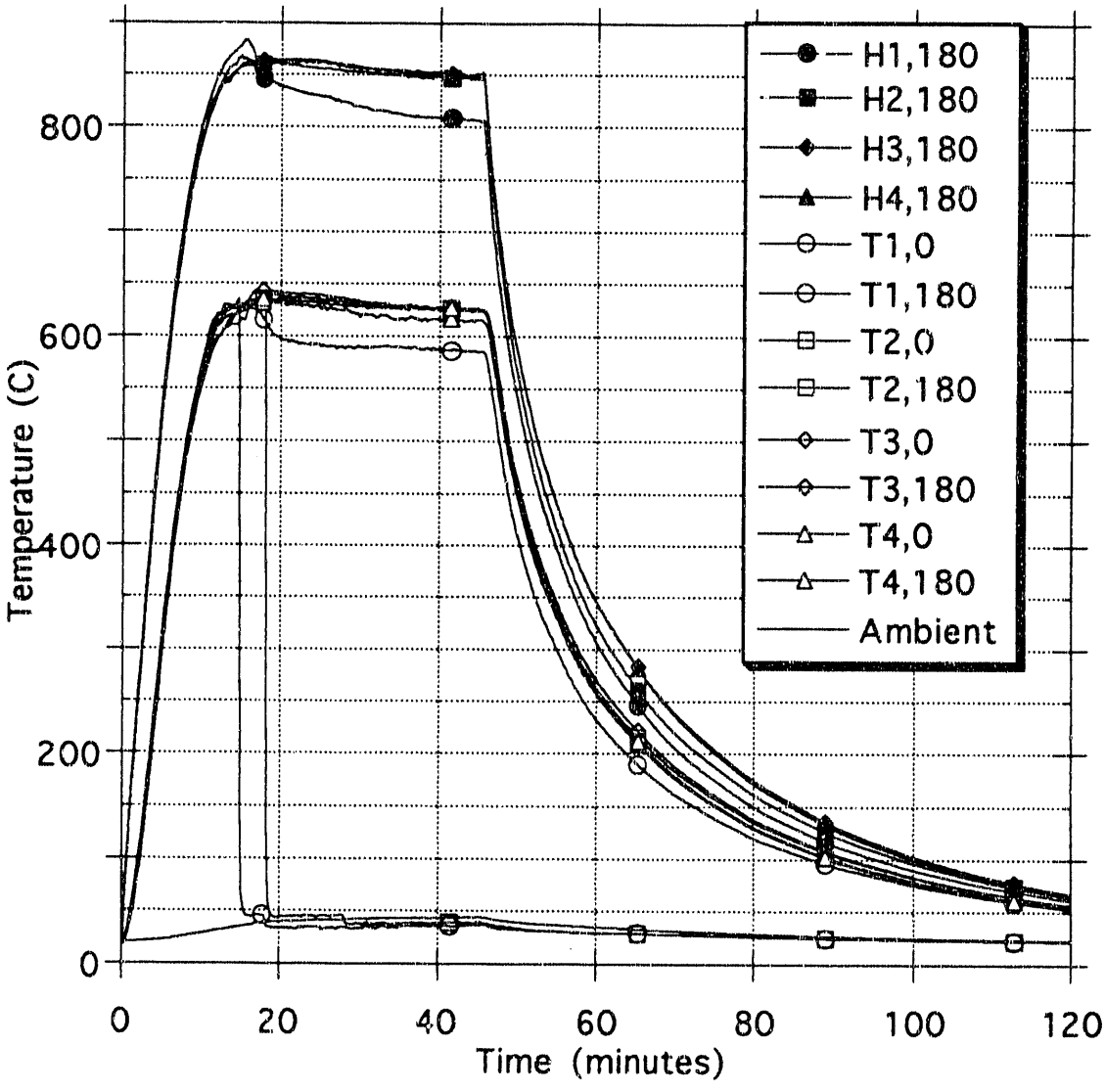

Figure 24. Heater and thimble temperatures for melt test of Test Series 4.

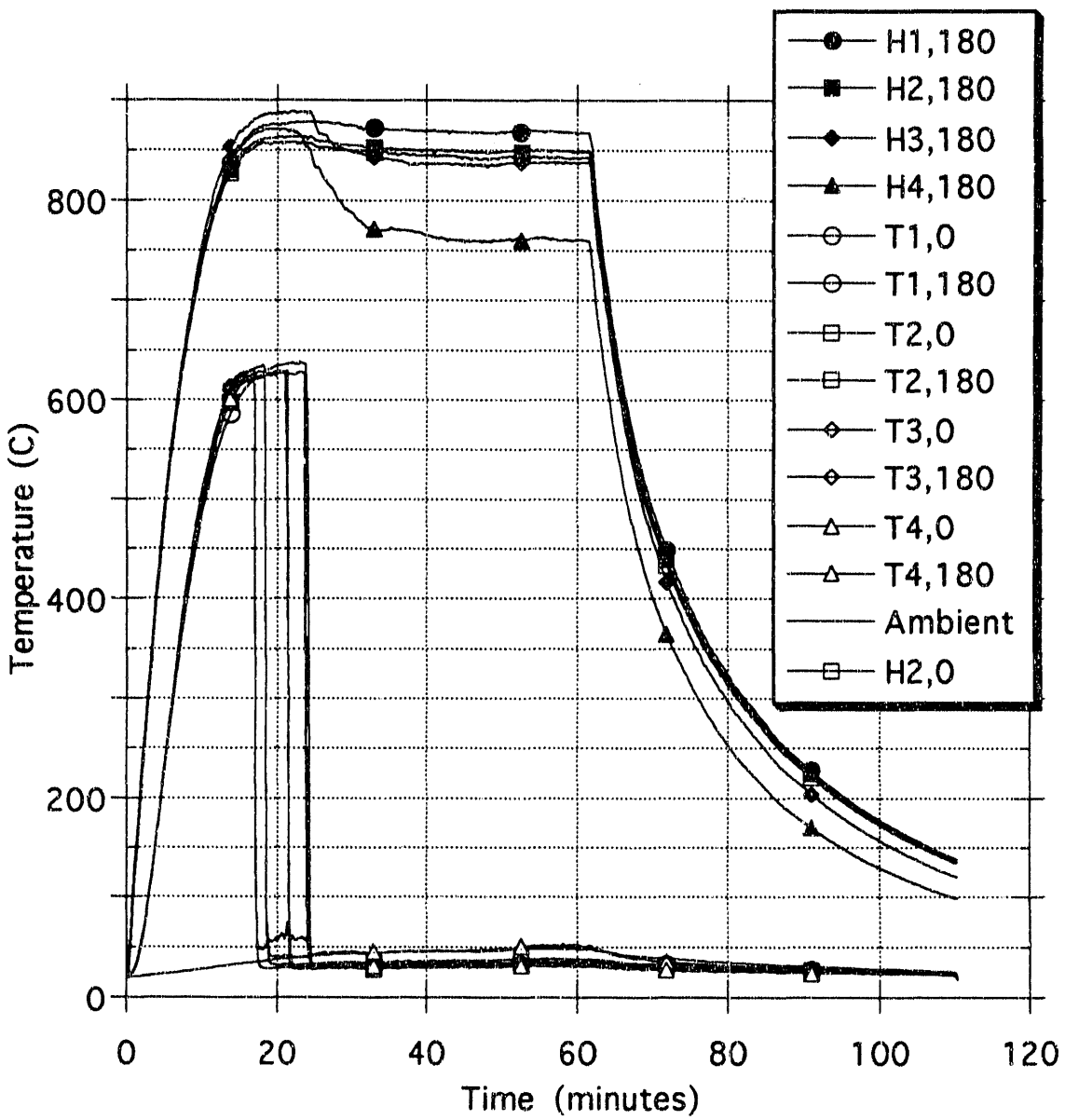

Figure 25. Heater and thimble temperatures for melt test of Test Series 5.

Figure 26. Results of the melt failure test of Test Series 3.

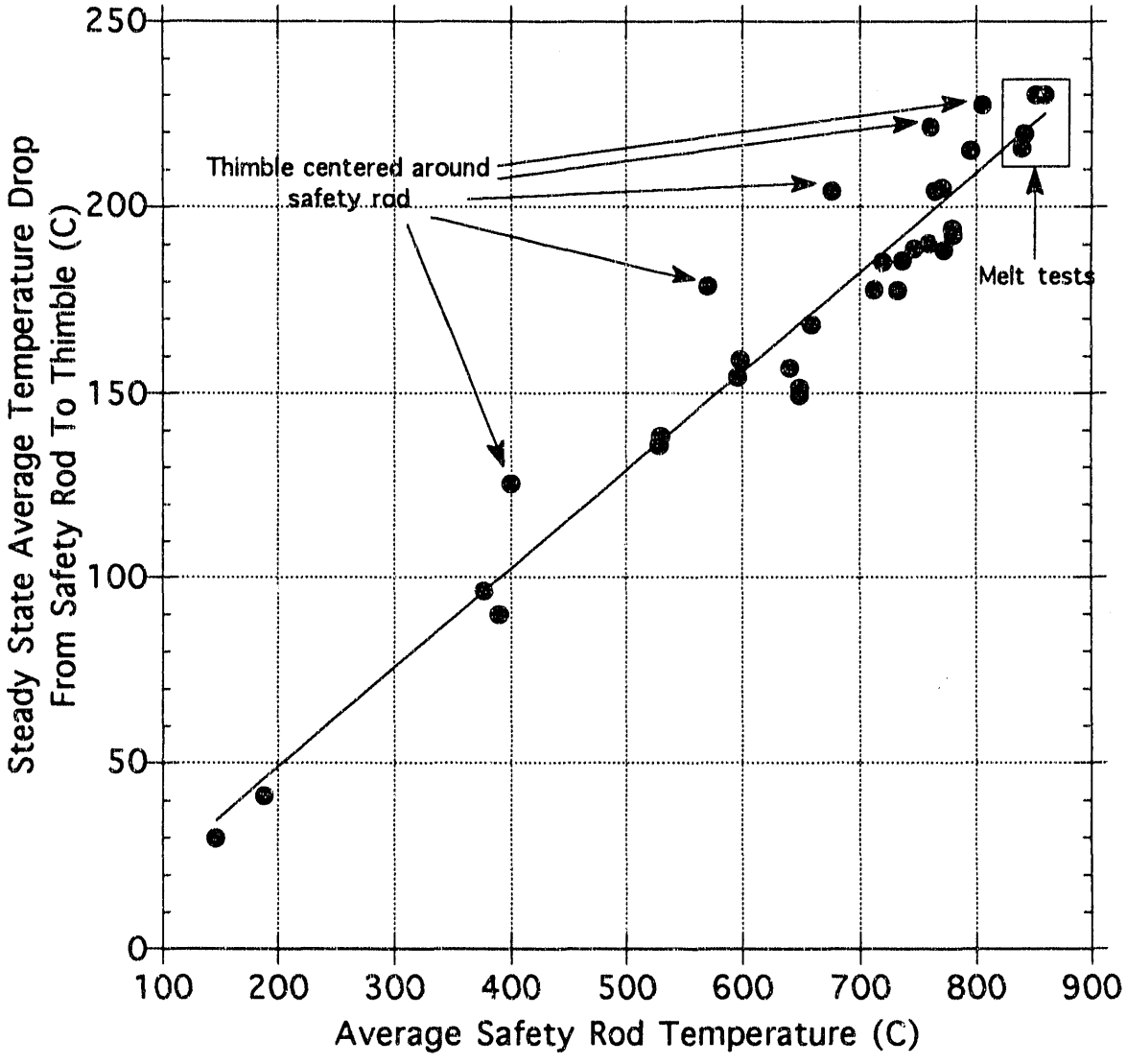

Figure 27. Steady state temperature drop from safety rod to thimble for various safety rod temperatures.

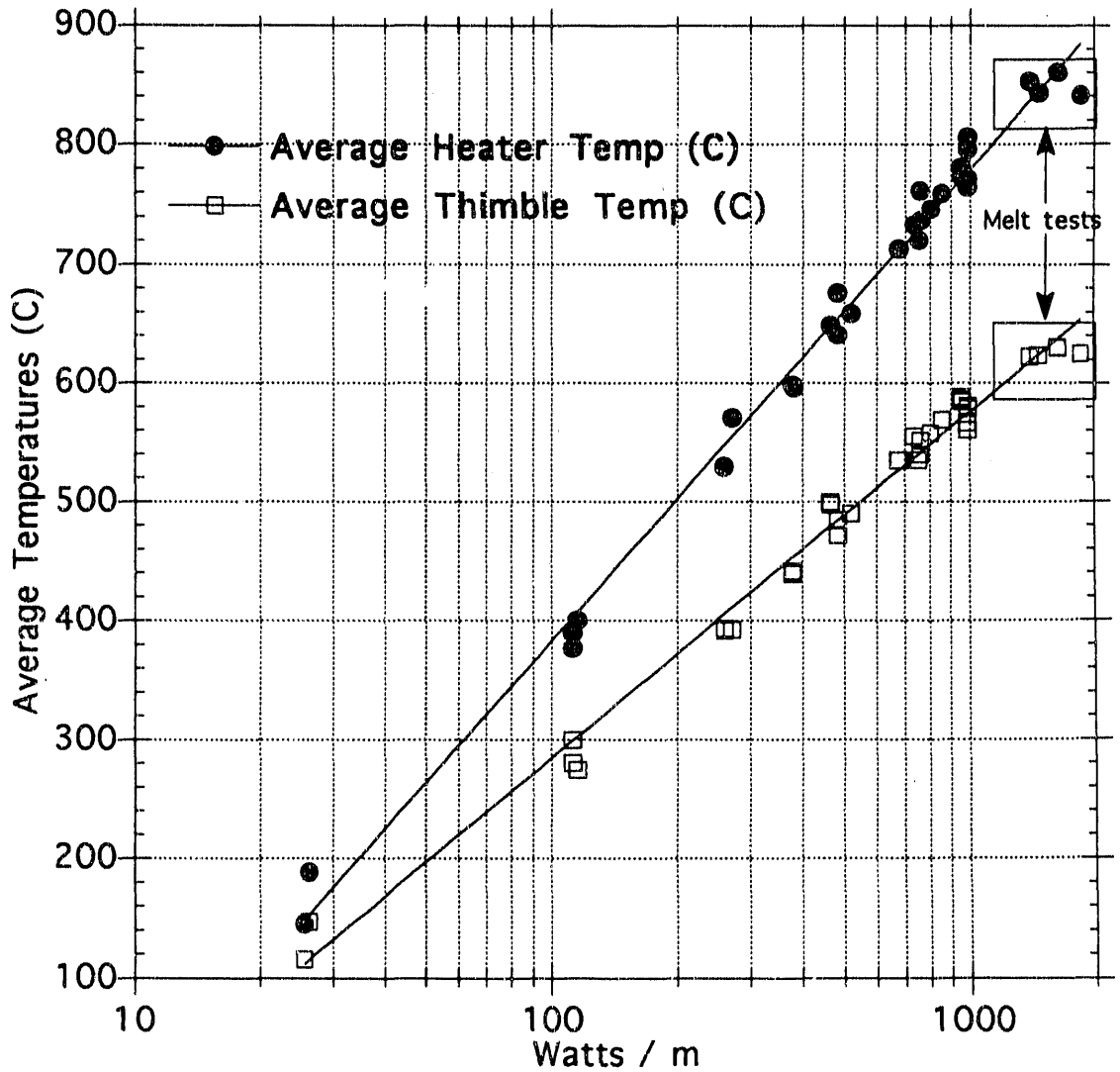

Figure 28. Average safety rod and thimble temperatures for various input power levels.

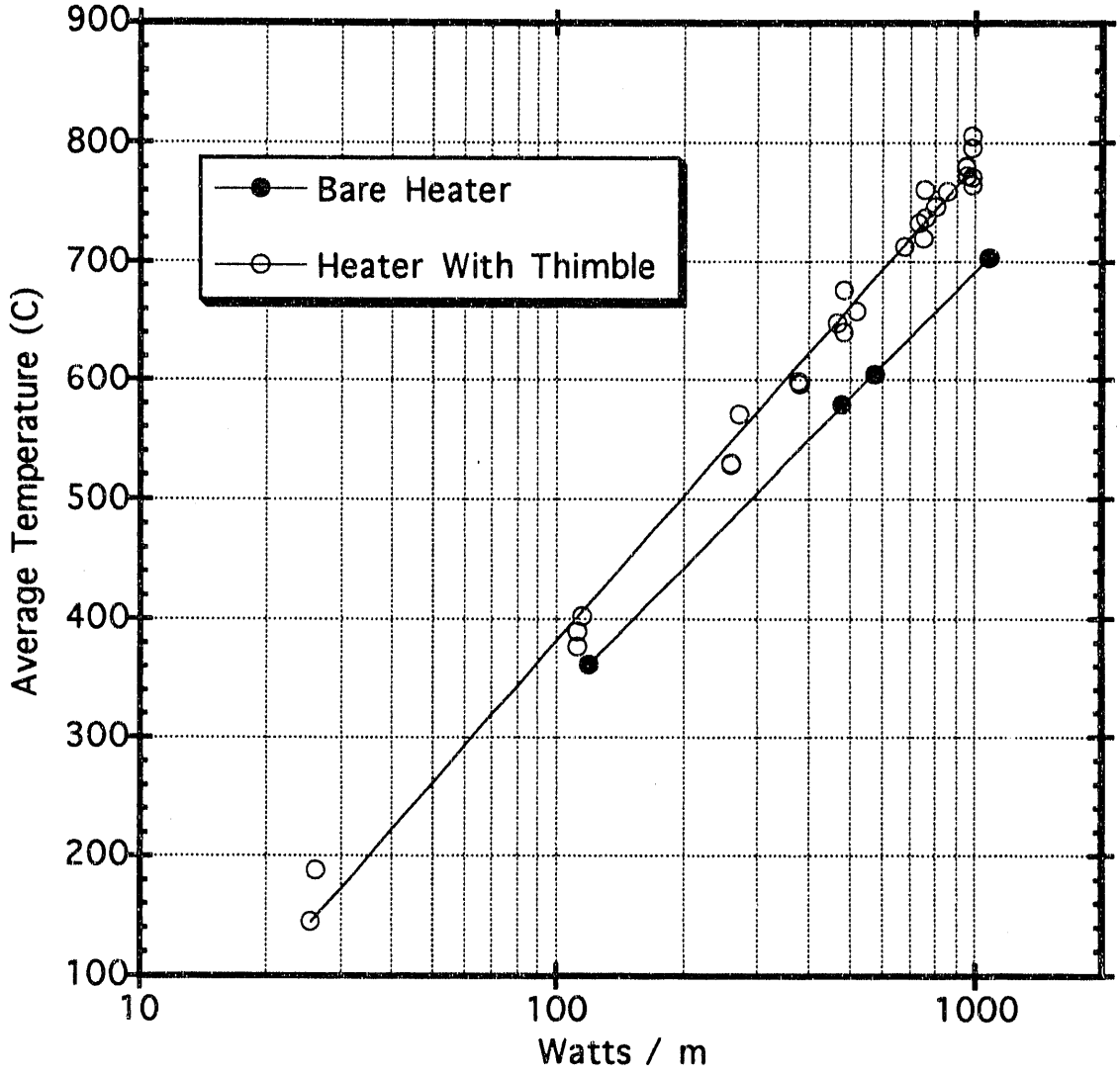

Figure 29. Comparison of simulated safety rod temperatures with and without a thimble.

APPENDIX A

NUMERICAL PREDICTIONS of HEAT TRANSFER for SRS SAFETY ROD/THIMBLE CONTACT EXPERIMENTS

NUMERICAL PREDICTIONS of HEAT TRANSFER for SRS SAFETY ROD/THIMBLE CONTACT EXPERIMENTS

A-1. INTRODUCTION

This appendix presents numerical studies performed in support of the experiments conducted to study the heat transfer and failure characteristics of a simulated SRS nuclear reactor safety rod/thimble assembly. These studies include heat transfer for a 2-D cross section of the heater/thimble assembly as shown in Figure A-1, and an axi-symmetric model of the bare heater to model the end effects of the heater apparatus as shown in Figure A-2. The 2-D cross section model is to verify the large temperature drop between the heater and the thimble and includes gray-body radiation between the heater and thimble. Various gap distances between the heater and the thimble are also modeled for experiment runs 4.4 and 5.5 from the main body of this report. The bare heater model used to model experiment run 1.4.

The numerical studies presented here were performed with the FIDAP [4] computer code. A description of FIDAP along with the model description is presented in Section A-2. The results are presented in Section A-3, along with the conclusions in Section A-4.

A-2. MODEL DESCRIPTION

The computer code FIDAP and the model description with heat transport equations and gray-body radiation assumptions are presented in this section.

A-2.1 FIDAP

FIDAP is a general purpose, three-dimensional computer aided computational fluid dynamics and heat transfer software package. It includes capabilities for generating finite element meshes in cartesian, cylindrical, or spherical coordinate systems, using automated command sequences. Element material properties, volumetric heat generation rates for elements, surface heat flux values and convection heat transfer coefficients for element faces may be specified. FIDAP was used to generate the finite

element meshes for the models described in this appendix. FIDAP was also used to solve the heat conduction-gray body radiation equations for the models. The FIDAP generated meshes were verified by inspecting the nodalization and boundary conditions prior to each use. FIDAP was also used as a post processor to view color contour plots and generate temperature line plots and mesh plots.

A-2.2 Problem Description

A 2-D cross section of the heater/thimble experiment is considered whose cross-sectional geometry is illustrated in Figure A-1. The calculation is performed in a cartesian coordinate system (x,y). The assumption is made that the temperatures in the entire model start at 10°C and a transient problem is run until the model converges on a steady state solution.

A-2.2.1 2-D Cross Section Model

As a result of electrically heating the Inconel, the heater assembly and thimble comes to steady state as described in the main body of this report. The governing equation of heat conduction in the heater assembly is given by

$$k\left(\frac{\partial^2 T}{\partial x^2}+\frac{\partial^2 T}{\partial y^2}\right)+Q(x,y,T)=0 \qquad \textbf{(A-1)}$$

and for the air and thimble is given by

$$k\left(\frac{\partial^2 T}{\partial x^2}+\frac{\partial^2 T}{\partial y^2}\right)=0 \qquad \textbf{(A-1a)}$$

where T(x,y) is the temperature, k is the thermal conductivity, and Q(x,y,T) is the heat source in the Inconel.

Boundary conditions for Equation A-1 are described as follows. The plane of symmetry through the bottom of the model is assumed to be adiabatic. The heat flux on the exterior surface of the thimble is given by

$$q = h[T_{th} - T_\infty] \qquad \text{A-2}$$

where T_{th} is the outside thimble temperature, T_∞ is the ambient room temperature, and h is the combined convective and radiative heat transfer coefficient, described as

$$h = h_c + h_r \qquad \text{A-3}$$

where h_C is the convective heat transfer coefficient and h_r is the radiative heat transfer coefficient. The convective heat transfer coefficient is given by the exact laminar boundary equations [5] for free convection on a vertical wall subjected to uniform surface temperature, described as

$$h_c = 0.508\left(\frac{k}{z}\right)Ra_z^{0.25}\left(\frac{Pr}{0.952 + Pr}\right)^{0.25} \qquad \text{A-4}$$

where Pr is the Prandtl number given by

$$Pr = \frac{\mu c_p}{k} \qquad \text{A-5}$$

where μ is the viscosity, c_p is the specific heat, and Ra_z is the local Rayleigh number given by

$$Ra_z = \frac{\rho^2 g\beta(T - T_\infty)z^3 Pr}{\mu^2} \qquad \text{A-6}$$

where z is the axial height along the heater, ρ is the density, g is gravitational acceleration, β is the volumetric expansion coefficient for air, given by

$$\beta = \frac{1}{T_f} \qquad \text{A-7}$$

where T_f is the film temperature, described as

$$T_f = \left(\frac{T + T_\infty}{2}\right). \qquad \text{A-8}$$

The air properties are evaluated at 12.5 psia and at the film temperature.

The applicable range for the laminar boundary equation correlation is valid for Rayleigh numbers below 10^9. The height used for this analysis is 0.508 m. which gives a Rayleigh number of 3.7×10^8 for a wall temperature of 600°C.

The radiative heat transfer coefficient is described as

$$h_r = \sigma \varepsilon_{th,eff} \left(T^2 + T_\infty^2\right)\left(T + T_\infty\right) \qquad \text{A-9}$$

where σ is the Stefan-Boltzman constant, and $\varepsilon_{th,eff}$ is the effective emissivity of the thimble. The effective emissivity of the thimble is calculated by combining the radiation from the outside of the thimble surface to the environment (T_∞), and the radiation from the inside of the thimble holes to T_∞. The effective emissivity is

$$\varepsilon_{th,eff} = 0.807\,\varepsilon_{th} \qquad \text{A-10}$$

where ε_{th} is taken from O'Brien's [6] emissivity measurements for aluminum alloy taken as

$$\varepsilon_{th} = 0.112 + 0.0000833(T - 300) \qquad \text{A-11}$$

where the temperature is in Kelvin.

The volumetric heat source in the Inconel Q(x,y,T) is calculated as follows. The amount of heat generated in the Inconel heater is decreased by the amount that is radiated from the surface of the stainless steel sheath through the holes to the environment. The resulting volumetric heat source in the Inconel is

$$q'''_{inc} = \frac{G\left(r_o^2 - r_i^2\right)_{inc} - 0.3307\,\varepsilon_{ss} D_{o,ss} \sigma\left(T_{ss}^4 - T_\infty^4\right)}{\left(r_o^2 - r_i^2\right)_{inc}} \qquad \text{A-12}$$

where G is the power input to the Inconel divided by the Inconel volume, 0.3307 is the view factor from the stainless steel sheath surface to the environment, ε_{ss} is the emissivity of the sheath, and D_o is the diameter of the sheath.

An effective emissivity of the stainless steel is used to account for the fraction of heat that is radiated directly through the holes in the thimble. This is calculated by multiplying the emissivity of the sheath by the fraction of the thimble that is solid compared to the total thimble area if the holes were not there. The resulting correlation is given by

$$\varepsilon_{ss,eff} = 0.6693\varepsilon_{ss} \qquad \text{A-13}$$

where ε_{SS} is taken at the lower error bands of the emissivity measurements made by O'Brien. The emissivity of the sheath is

$$\varepsilon_{ss} = 0.15 + 0.0001(T_{ss} - 300) \qquad \text{A-14}$$

where T_{SS} is the stainless steel temperature in Kelvin.

The gray body radiation heat flux boundary condition on the stainless steel surface and on the inside of the thimble is described as

$$\sum_{j=1}^{N}\left(\frac{\delta_{ij}}{\varepsilon_j} - F_{ij}\frac{1-\varepsilon_j}{\varepsilon_j}\right)q_j = \sum_{j=1}^{N}\left(\delta_{ij} - F_{ij}\right)\sigma T_j^4 \qquad \text{A-15}$$

where q_j is the radiative heat flux and T_j is the temperature of the j'th surface, δ_{ij} is the Kronecker delta and ε_j is the emissivity of the j'th surface, and F_{ij} is the view factor given by

$$F_{ij} = \frac{1}{A_i}\int_{A_i}\int_{A_i}\frac{\cos\beta_i \cos\beta_j dA_i dA_j}{\pi r^2} \qquad \text{A-16}$$

where A_i and A_j are the areas of surfaces i and j, respectively, and β_i and β_j are the angles between the position-dependent normal vectors to surfaces i and j in a line of length r connecting the points of evaluation of the normals. The emissivity on the

inside surface of the thimble is the same as Equation A-11. The emissivity of the air surfaces along the plane of symmetry is taken as 0.001, a very small value to approximate near perfect reflection of the heat along those surfaces.

A-2.2.2 Axi-symmetric Bare Heater Model

The axi-symmetric bare heater model as shown in Figure A-2 is described in the following section. The copper blocks used to conduct the electricity from the cables to the Inconel are assumed to be disks with the same surface area and volume as the blocks. The governing equation of heat conduction for the bare heater model is

$$\frac{1}{r}\frac{\partial}{\partial r}\left(kr\frac{\partial T}{\partial r}\right)+\frac{\partial}{\partial z}\left(k\frac{\partial T}{\partial z}\right)+Q=0 \qquad \text{A-17}$$

where T(r,z) is the temperature, Q is the volumetric heat source in the Inconel, and k is the thermal conductivity of the appropriate material. Heat flux boundary conditions for the bare heater are the same as the outside of the thimble as described earlier with the exception of the heater emissivity being the same as Equation A-14. A convective heat transfer coefficient of 3.0 W/m^2-K and an emissivity of 0.5 is applied to the copper blocks for the black body radiation heat flux.

A-2.3 Material Properties

The material properties of the various components used in this analysis are given by [7,8]

Material	Thermal Conductivity (W/m-K)
Aremcolox	15.6
Inconel 600	11.7
Nickel-Aluminum	20.0
Alumina-Titania	2.0
Stainless Steel 304	18.0
Air	0.03-0.05 (varies with temperature)
Thimble	105.0

The conductivity of the thimble is normally taken at 150 W/m-K, but taking into account the holes the effective thermal conductivity is 105 W/m-K.

A-3. RESULTS

This section describes the results of the numerical calculations for the 2-D cross section model and the axi-symmetric bare heater model.

A-3.1 2-D Cross Section Model

The finite element mesh used for the 2-D cross section model for the case with the thimble centered around the heater is shown in Figure A-3. Nine noded quadrilateral elements were used in the model to represent the experimental test run 5.6. Temperature contours are shown in Figure A-4 for the centered case. The largest temperature drop occurs across the air gap since air has such a low thermal conductivity compared to the other materials. The maximum temperature in the heater is 747°C and the minimum (thimble) temperature 588°C. Temperatures measured during the experiment were 780°C, and 580°C respectively. Good agreement exists between the experimental and analytical results for this centered model.

Figure A-5 shows the finite element mesh for the case where a 0.0254 mm gap exists between the thimble and the heater. This model is used to predict the temperature distribution for experimental run 4.4, which had contact at the top and bottom of the thimble. After the experiment was completed it appears that the thimble bowed away from the heater along the starting contact line. The next two models show the temperature distribution with different gap thicknesses. The mesh is graded towards the point of contact to help more accurately calculate the azimuthal temperature profile. Temperature contours are plotted in Figure A-6 for the 0.0254 mm gap. The maximum temperature is 683°C in the heater on the opposite side of the point of contact, while the minimum temperature is 601°C in the thimble, also 180° opposite the nearest point of contact. These temperatures correspond to the experimental temperatures of 760°C and 550°C. The temperature difference between the experiment and the analysis is about 70°C. Models were set up and run for gaps of 0.254 mm, 0.381 mm, and 0.635 mm in order to assess the sensitivity of the temperature distribution to the gap distance.

The finite element mesh for the 0.635 mm gap is shown in Figure A-7. Temperature contours are shown in Figure A-8 for the 0.635 mm gap model. The results are in-between the centered case and the very small gap case. The average heater temperature is 725°C, while the thimble average temperature is 586°C. These temperatures correspond more closely with the measured temperatures in the experiment of 760°C and 550°C, which shows about a 30°C temperature difference. Figure A-9 shows the azimuthal temperature profile of the stainless steel sheath. The 0.0254 mm gap has the largest azimuthal temperature difference of 32°C and the 0.635 mm gap has the smallest temperature difference of 9°C. Figure A-10 shows the azimuthal temperature drop of the thimble. Again the 0.0254 mm gap has the largest drop of 20°C, while the 0.635 mm gap model shows only a 9°C temperature drop. These azimuthal temperature variations agree well with the experimental temperature variations. The measured temperature difference between the front and back of the heater for run 4.4 was approximately 25°C, depending on the height. The azimuthal temperature difference of the thimble was measured at about 12°C.

A-3.2 Axi-Symmetric Bare Heater Model

The finite element mesh used for the bare heater axi-symmetric model is shown in Figure A-11. The full mesh is shown along the bottom with an expanded view of the bottom end shown above. This finite element mesh was created to model experiment run 1.4. Temperature contours are shown in Figure A-12 of the bare heater model. There exists a large temperature drop along the assembly towards the top and bottom ends. Figure A-13 shows the predicted axial temperature profile compared with the measured temperatures. The temperature difference between analytical and experimental is relatively small. The FIDAP predicted temperature profile shows the dependence on the convective heat transfer coefficient as it decreases along the heater as the boundary layer thickness grows.

A-4. CONCLUSIONS

Finite element models have been created to model heat transport with convective and radiative boundary conditions for the 2-D cross section of the heater-thimble model, and the axi-symmetric bare heater model with end effects. Gray body radiation boundary conditions are also used for the 2-D cross section model.

A large temperature drop of 160°C across the air gap between the heater and the thimble was predicted with the numerical calculations for the case where the heater is centered in the thimble. The predicted temperature in the heater is 80°C lower than the measured temperature in the experiment, and the predicted thimble temperature is 50°C higher. These values are relatively small compared to the magnitude of the predicted temperatures and considering a two dimensional model is being used to represent a three dimensional situation.

Four models were created with different gap spaces between the heater and the thimble for the 2-D cross section geometry. The gap distances varied from 0.0254 mm to 0.635 mm The small gap predicted lower heater temperatures and higher thimble temperatures than were measured. As the gap is increased the difference between the predicted and measured temperatures for the heater and thimble decreases.

An axi-symmetric bare heater model was created to show the axial temperature distribution. By using the emissivity at the lower limits of the measured error bands, and applying the exact laminar boundary layer equations for natural convection along a flat plate, the FIDAP predicted temperatures agree with the measured experimental temperatures.

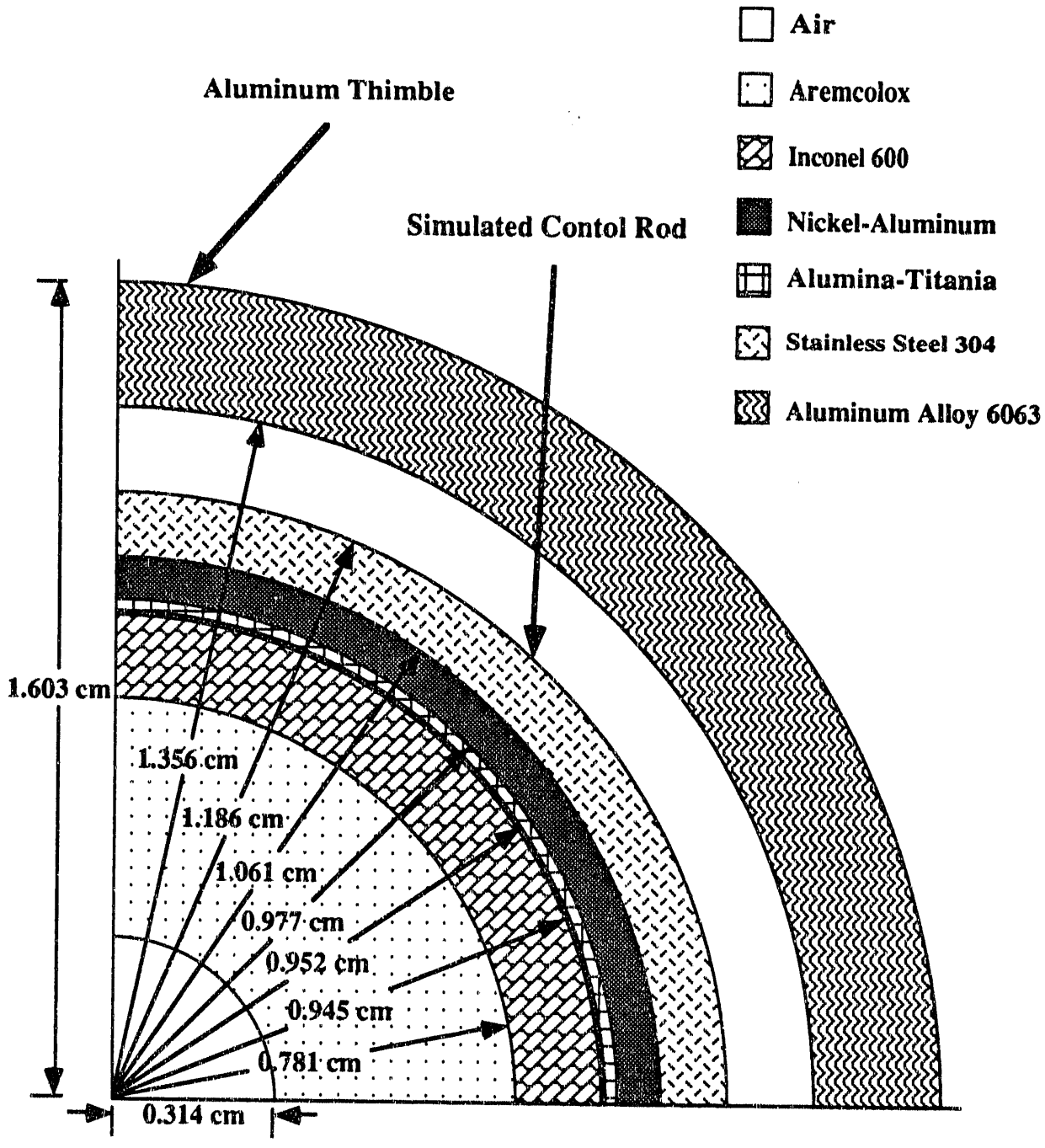

Figure A-1 2-D cross sectional geometry of heater/thimble.

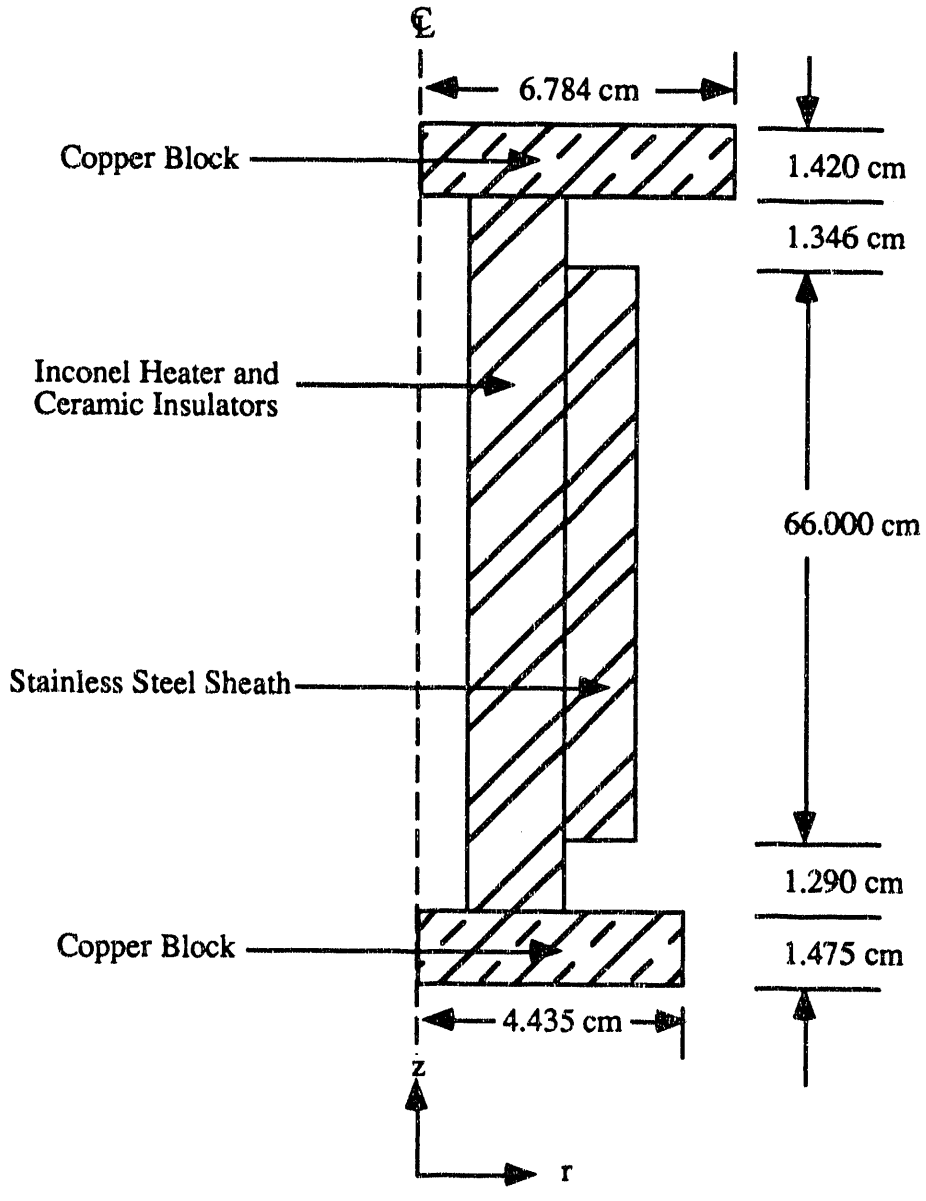

Figure A-2 Axi-symmetric geometry of bare heater

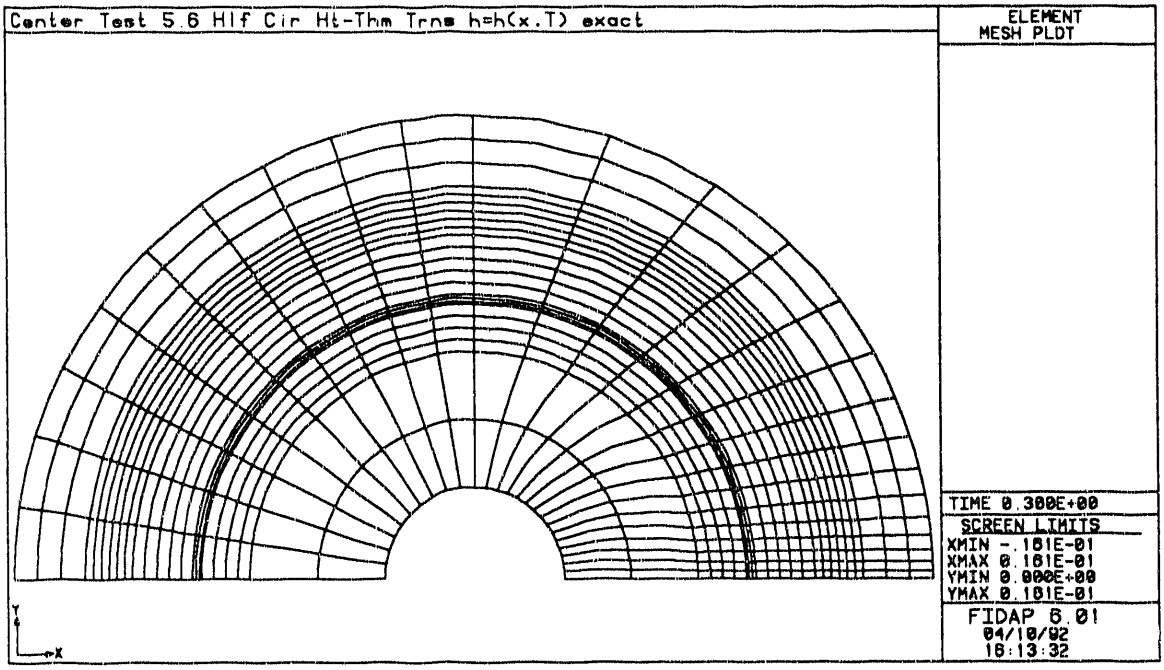

Figure A-3 Finite element mesh for centered model.

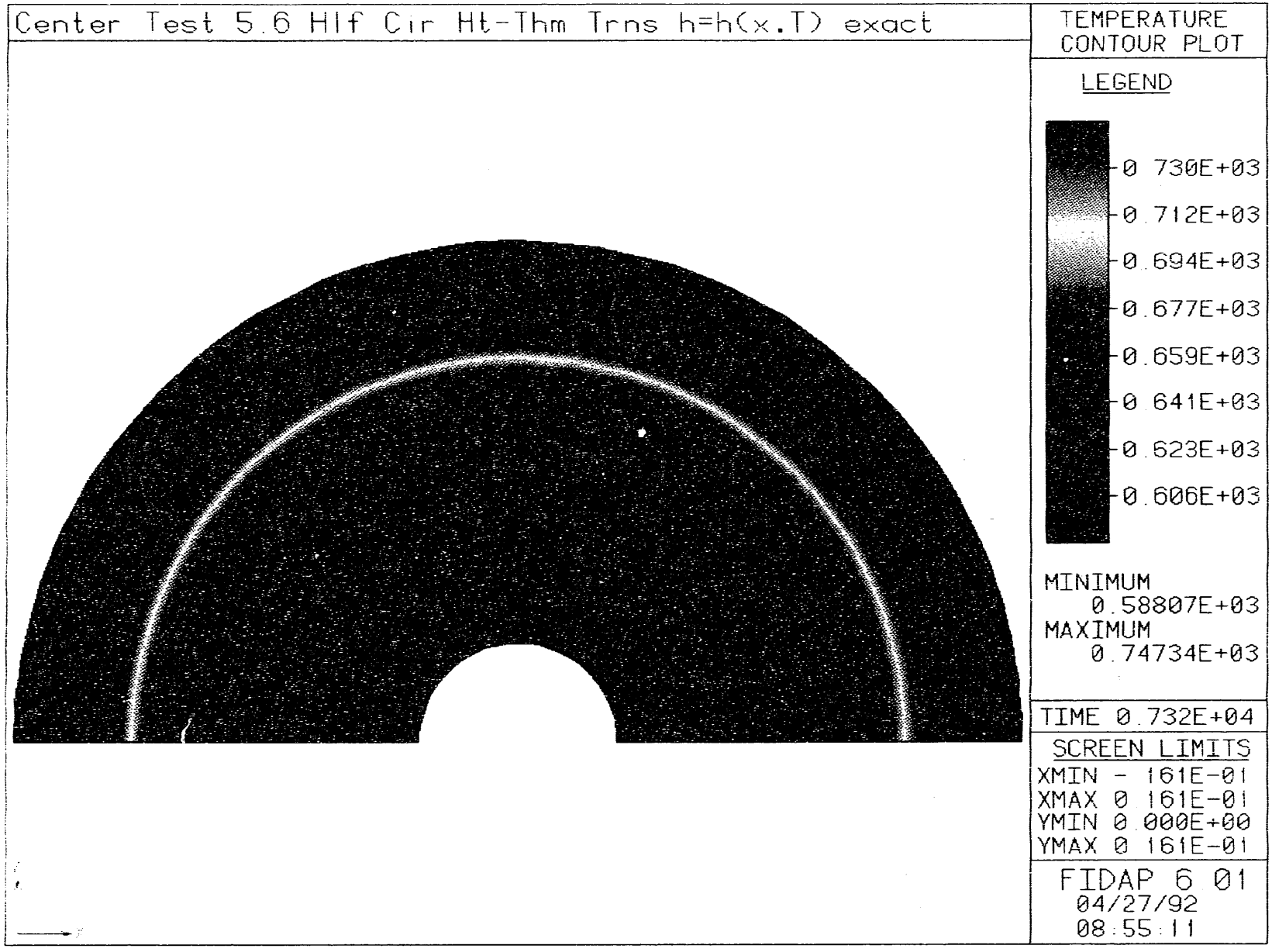

Figure A-4 Temperature contours for centered model.

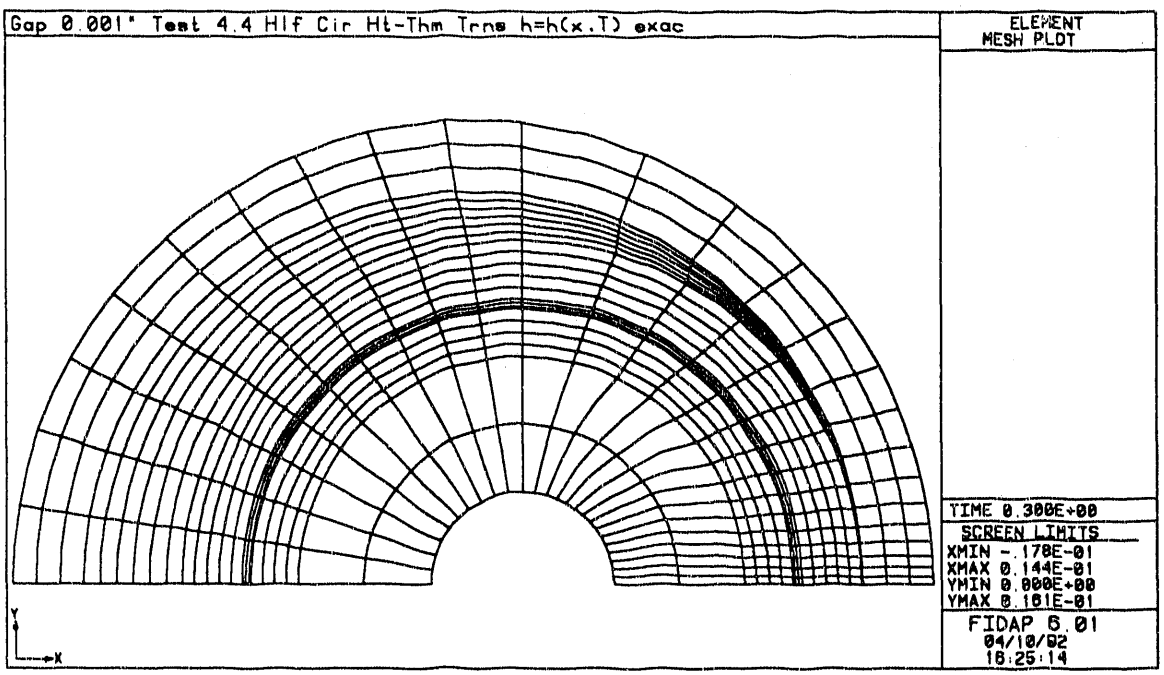

Figure A-5 Finite element mesh for 0.0254 mm gap model.

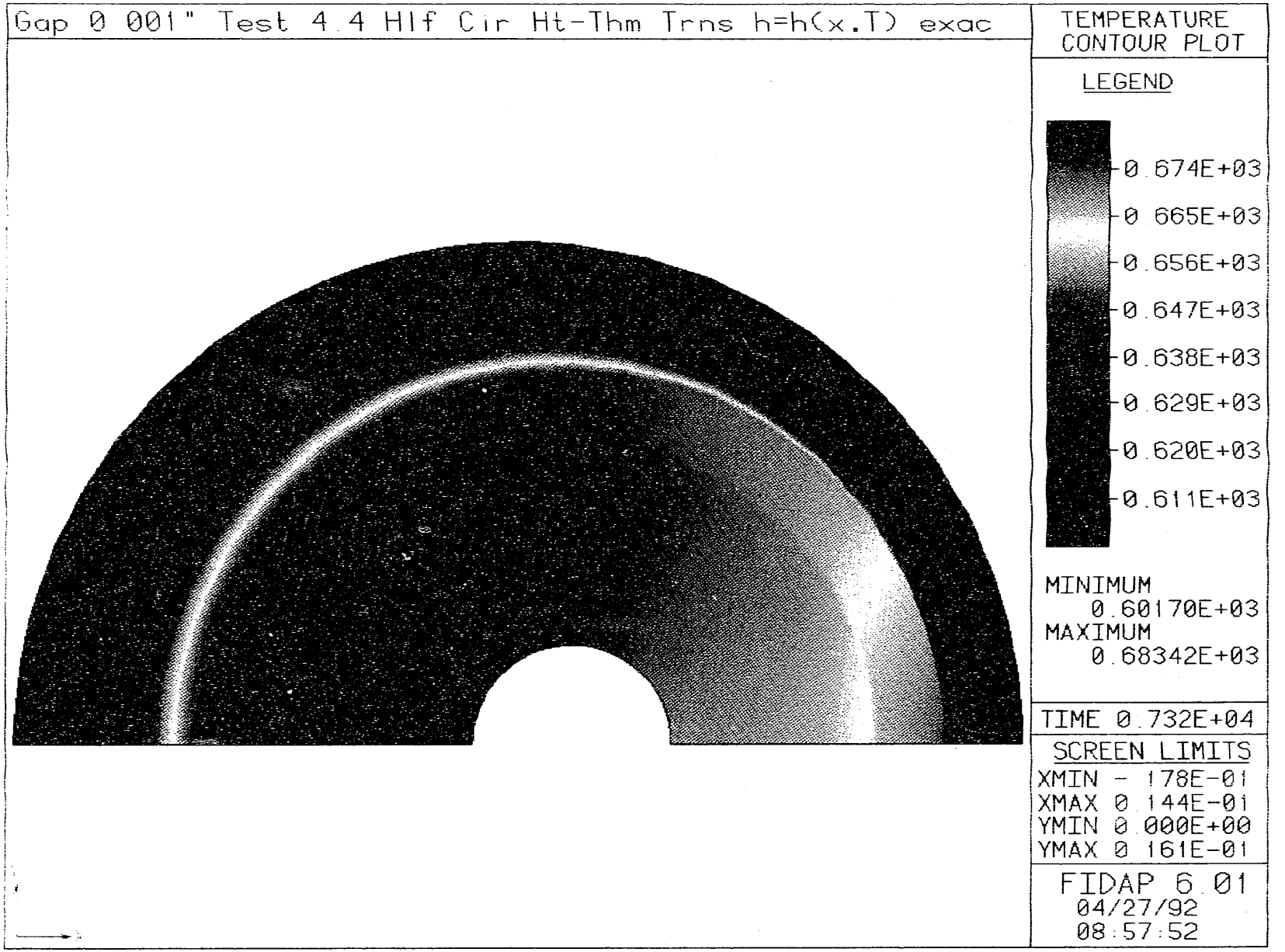

Figure A-6 Temperature contours for 0.0254 mm gap model.

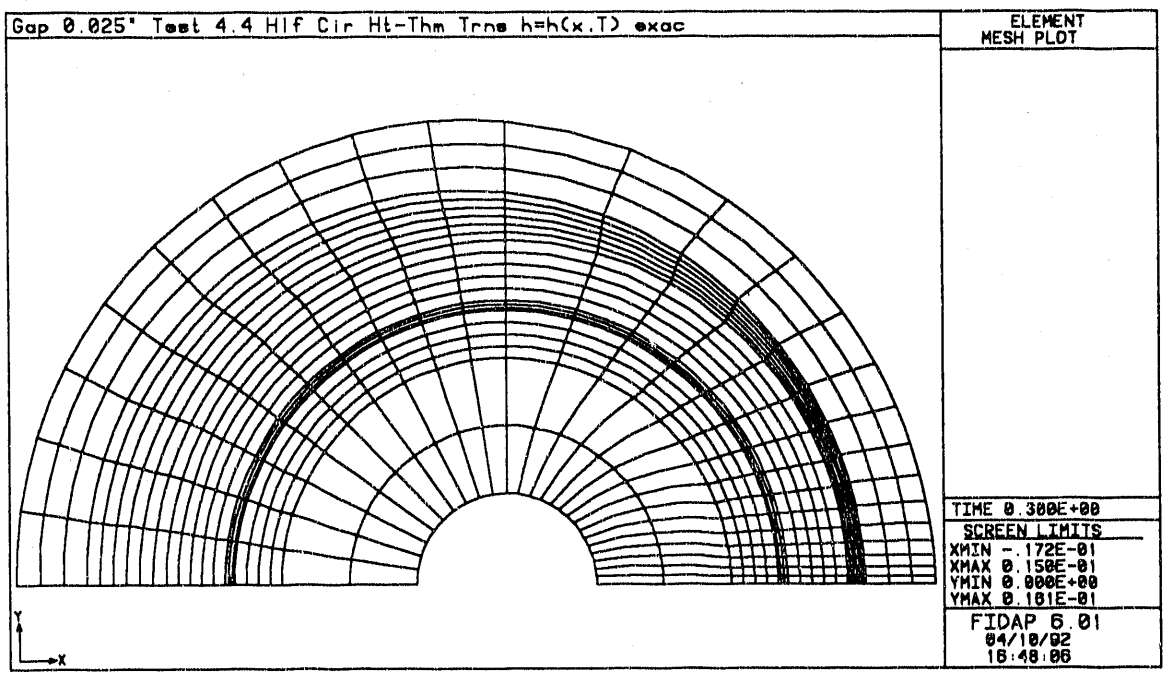

Figure A-7 Finite element mesh for 0.635 mm gap model.

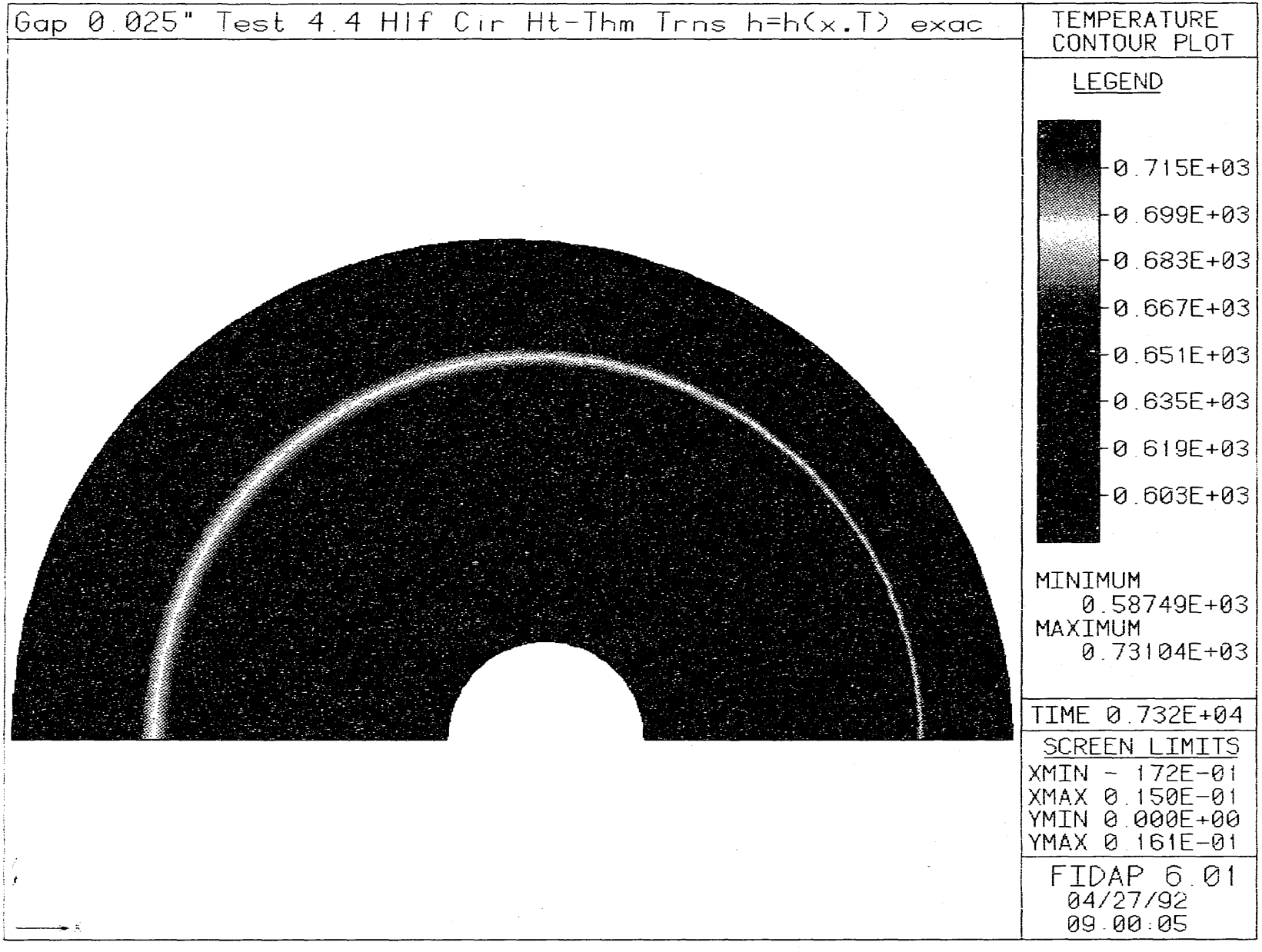

Figure A-8 Temperature contours for 0.635 mm gap model.

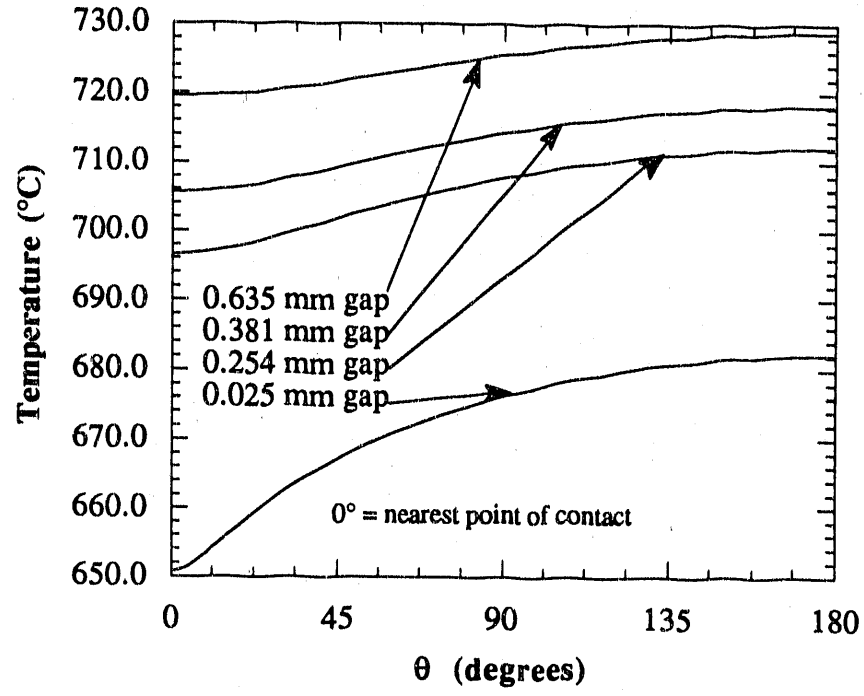

Figure A-9 Azimuthal temperature profile for stainless steel.

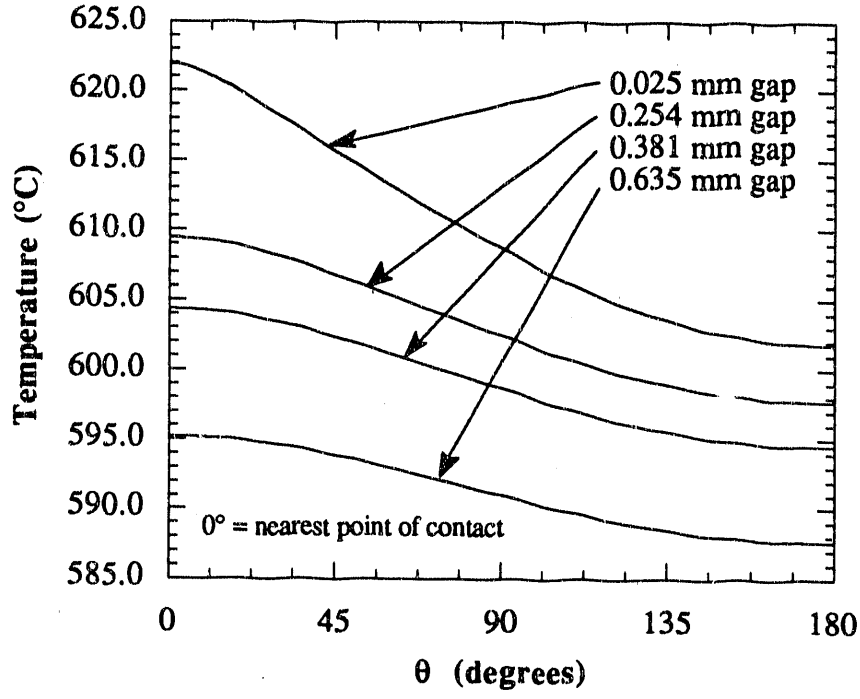

Figure A-10 Azimuthal temperature profile for thimble.

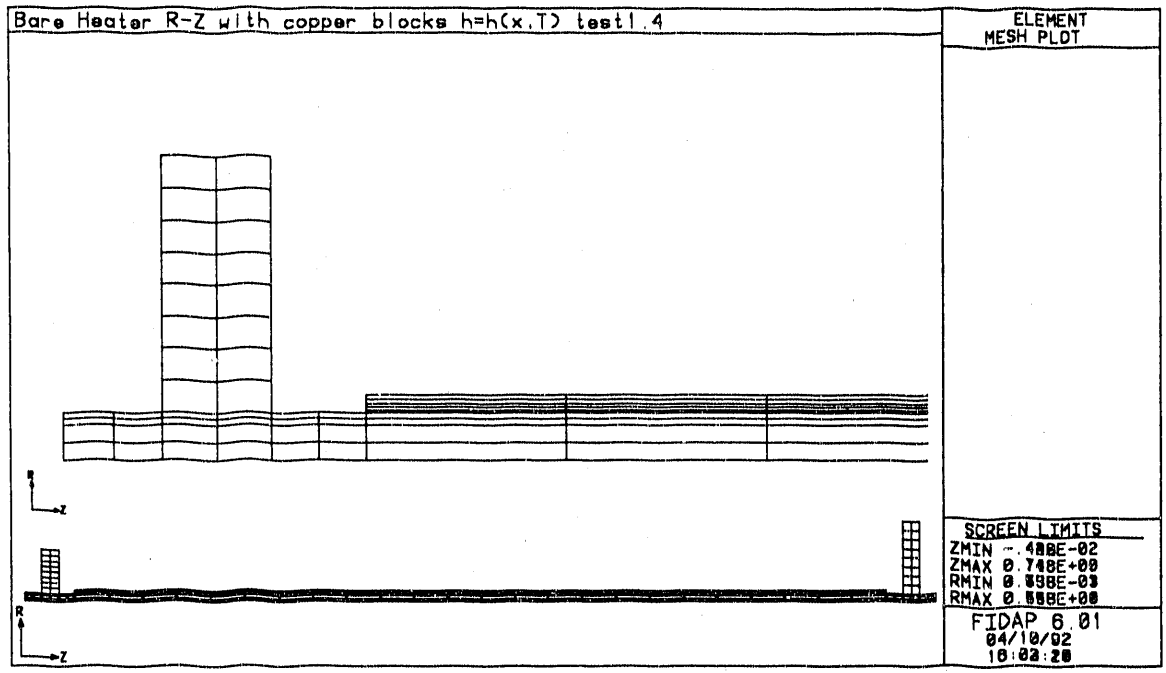

Figure A-11 Finite element mesh for axi-symmetric bare heater model.

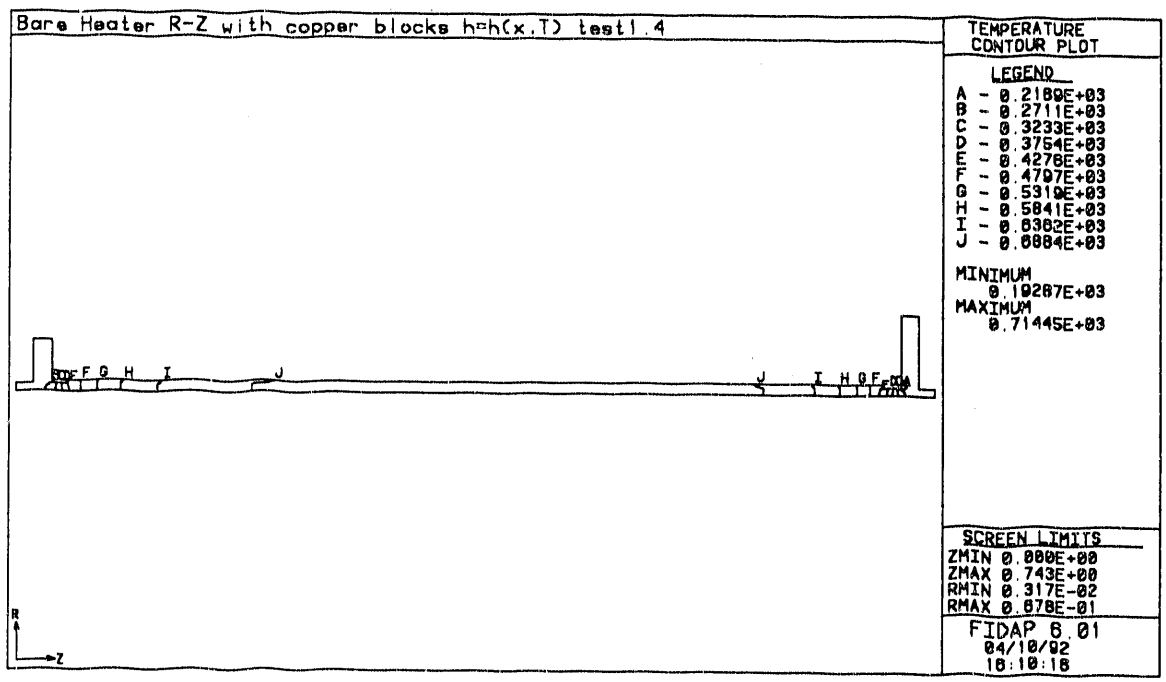

Figure A-12 Isotherms for bare heater model.

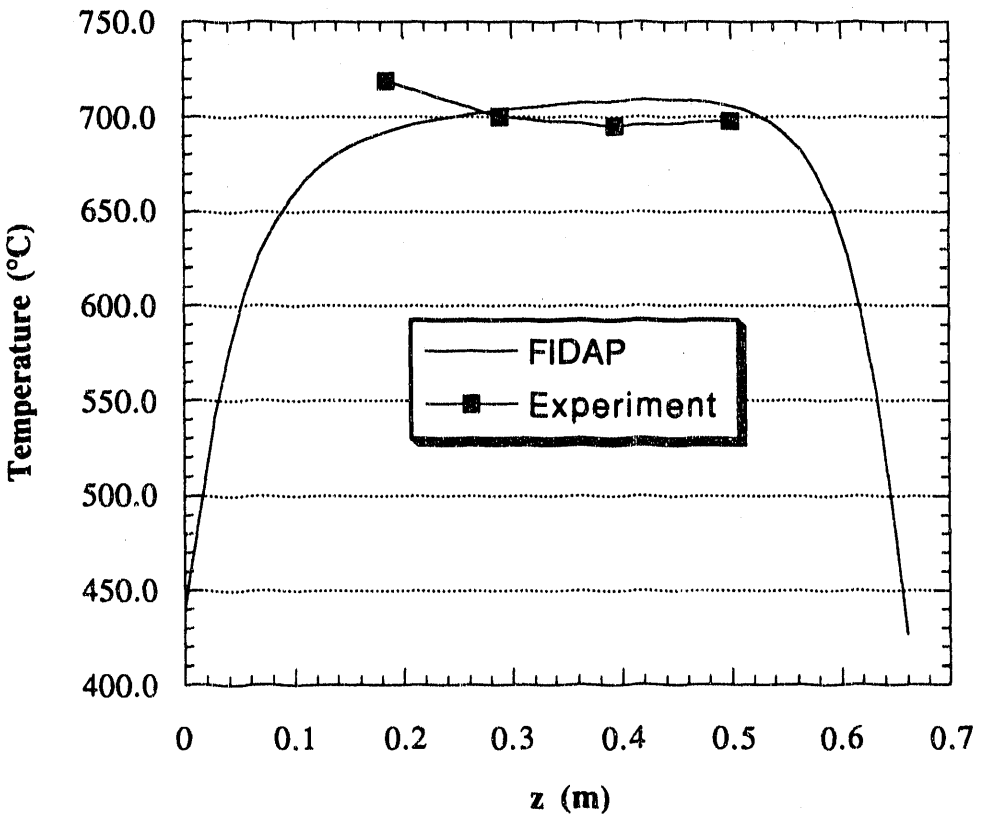

Figure A-13 Predicted vs measured axial temperatures for bare heater model.

END

DATE FILMED

8/26/92